Materials Science & Engineering A 803 (2021) 140696

Contents lists available at ScienceDirect

Materials Science & Engineering A

journal homepage: http://www.elsevier.com/locate/msea

Review article

The influence of stacking faults on mechanical behavior of advanced materials

Ruizhe Su [a], Dajla Neffati [b], Yifan Zhang [a], Jaehun Cho [a], Jin Li [c], Haiyan Wang [a], Yashashree Kulkarni [b], Xinghang Zhang [a,*]

[a] School of Materials Engineering, Purdue University, West Lafayette, IN, 47907, USA
[b] Department of Mechanical Engineering, University of Houston, Houston, TX, 77204, USA
[c] Institute of Special Environments Physical Sciences, Harbin Institute of Technology, Shenzhen, China

ARTICLE INFO

Keywords:
Stacking faults
Twin
In situ
Molecular dynamics
Mechanical property

ABSTRACT

There are abundant studies on deformation mechanisms in metallic materials dominated by grain boundaries and twin boundaries. In comparison, the influence of stacking faults on deformation mechanisms of materials remains less well understood. Recent studies have shown that when the density of stacking faults increases sharply, their influence on mechanical behavior of metallic or ceramic materials becomes prominent, and in fact, dominates in some cases. This article reviews recent research progress on how nanoscale stacking faults impact the mechanical behavior of metallic and ceramic materials. We primarily focus on studies that reveal the formation of pre-existing stacking faults, their interactions with dislocations, and phase transformations during plastic deformation as evidenced by experiments and simulations. The aim of this review is to highlight the potential opportunities in using stacking faults to tailor the deformation mechanisms of advanced materials.

1. Introduction

Twin boundaries (TBs) and stacking faults (SFs) are common planar defects in face-centered cubic (FCC) and hexagonal close packed (HCP) metals. Lu et al. revealed high-density TBs in nanotwinned Cu enhanced the strength of Cu while retaining good ductility [1]. Simultaneously Zhang et al. showed that TBs in nanotwinned stainless steels were effective barriers to the transmission of dislocations [2]. Since then, extensive studies have focused on the fabrication of nanotwinned metals, and understanding their mechanical behavior via both experiments and simulations [2–43]. It has been shown that TBs not only strengthen the materials, but also emit mobile dislocations, and thus permit good plasticity and work hardening ability in nanotwinned metals [1,12,15,18,30–32,37,38,44–52].

Although SFs were frequently observed in various metallic materials, the effects of high-density SFs on mechanical behavior received less attention in comparison to TBs. FCC and HCP metals with low stacking fault energy (SFE) or nanoscale grain size tend to form SFs during plastic deformation. However, it is difficult to investigate the role of SFs on mechanical behavior because most SFs formed after plastic yielding. Recently, several metallic and ceramic materials with abundant pre-existing SFs were fabricated, providing good opportunities to investigate the relationship between SFs and mechanical behavior. In this review article, we will summarize the current views on the significance of SFs on mechanical behavior of metallic and ceramic materials and discuss unresolved issues for future studies.

2. Fabrication and microstructure of metals and ceramics with pre-existing SFs

SF is a planar defect that consists of atomic layers with altered stacking sequences, mostly found in close-packed crystal structures. SFs that are formed by vacancy agglomeration are named as intrinsic SFs and others produced by interstitial agglomeration are named as extrinsic SFs (Fig. 1a) [53]. Metals with low-to-medium SFE can form high-density SFs easily during a non-equilibrium process like magnetron sputtering [3,54–60] or, by plastic deformation such as ball milling [61], rolling [62–64], surface engineering [65,66], torsion [67], and tensile deformation [68,69]. Co films deposited on Cu seed layer grew epitaxially and contained high-density SFs [54,56]. Inclined and intercepting SFs in FCC (100) Co had an average spacing of 25 nm on different sets of {111} planes (Fig. 1b), nucleating from the Cu/Co interface due to the

* Corresponding author.
E-mail address: xzhang98@purdue.edu (X. Zhang).

https://doi.org/10.1016/j.msea.2020.140696
Received 17 July 2020; Received in revised form 17 December 2020; Accepted 19 December 2020
Available online 6 January 2021

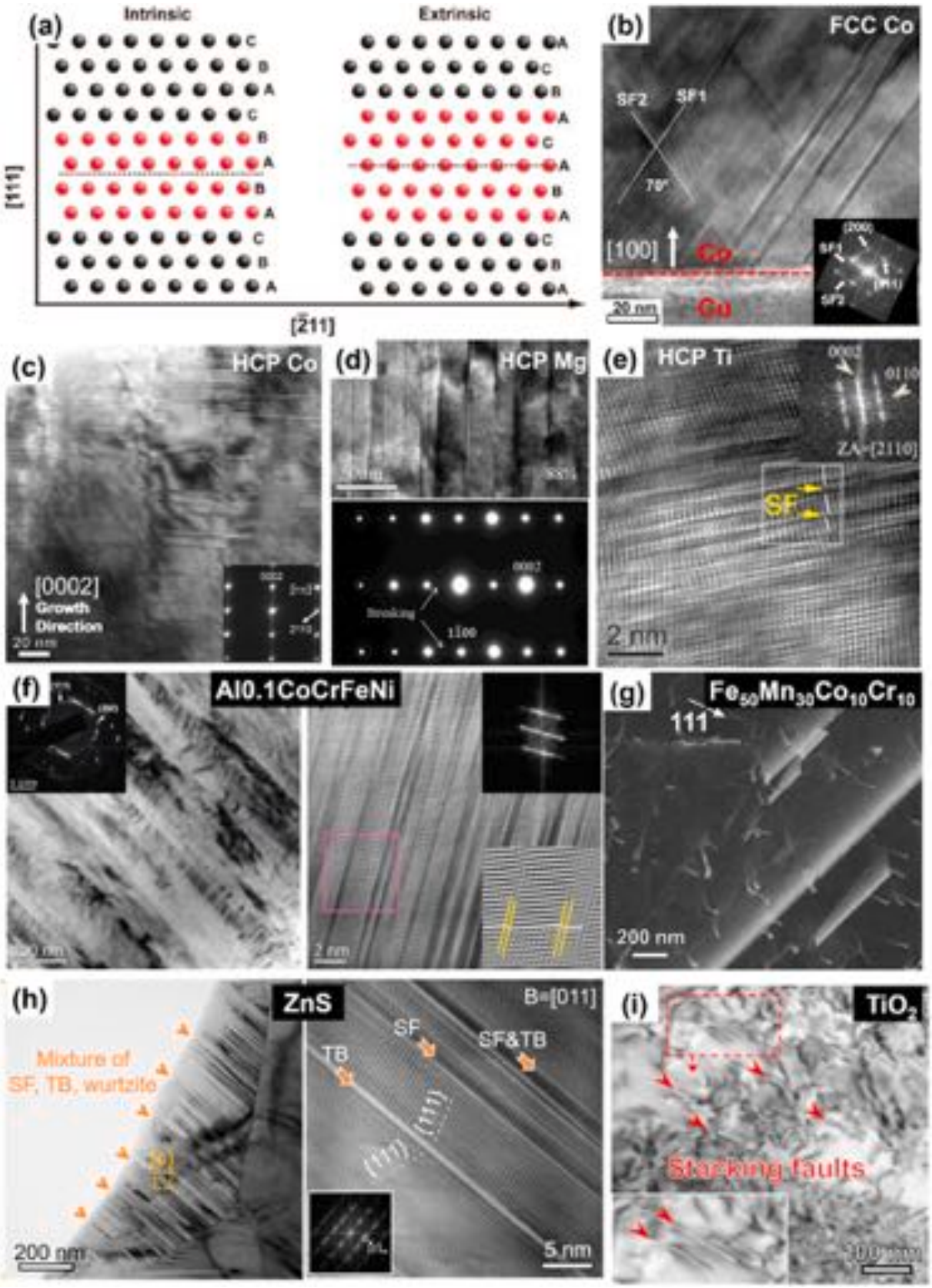

Fig. 1. (a) Schematic of intrinsic and extrinsic SFs in FCC structure [53]. (b) Inclined SFs on different (111) planes in FCC Co thin film [56]. (c) Parallel SFs on basal planes in HCP Co thin film [54]. (d) SFs on basal plane in Mg alloys after hot rolling to 88% strain [63]. (e) SFs in nanocrystalline Ti thin film [59]. (f) Nanoscale SFs in $Al_{0.1}CoCrFeNi$ high entropy alloys [58] (g) Dark field TEM micrograph showing SFs in $Fe_{50}Mn_{30}Co_{10}Cr_{10}$ [64]. (h) Bright field TEM image of a grain with a high density of SFs and TBs in ZnS [79]. (i) Bright-field TEM micrograph showing an area of the flash-sintered TiO_2 containing SFs [80].

lattice mismatch strain. The high-density SFs in Co (100) also stabilized the FCC phase at room temperature. In HCP Co (0002), parallel SFs formed on basal planes, with an average SF spacing of 9 nm (Fig. 1c). In Mg alloys, SFs on basal planes became the dominant defects when sample thickness reduction by hot rolling exceeded 50%, and the SF spacing decreased to 16 nm after 88% of thickness reduction (Fig. 1d) [63]. In addition to the applied shear stress during hot rolling, the decrease in the SFE induced by Y and Gb solutes [70,71] also promoted partial dislocation migration and SF formation in Mg alloys [63]. High-density SFs were also observed in sputtered nanocrystalline Ti thin films (Fig. 1e) [59]. SFs have also been reported in some high entropy alloys due to their low SFE [58,60,64,72–77]. In $Al_{0.1}CoCrFeNi$, a low deposition rate promoted nanoscale TB formation, while a high deposition rate induced nanoscale SFs (Fig. 1f) [58]. Interestingly, previous studies showed that a higher deposition rate promoted the formation of TBs in nanotwinned metals [78]. The influence of deposition rate on the formation of TBs versus SFs needs more investigations. In dual-phase high entropy alloys, such as $Fe_{50}Mn_{30}Co_{10}Cr_{10}$, SFs with various thickness were also observed after water quench (Fig. 1g) [64].

In general, compared with metals, SFs are rarely observed in most ceramics because the dislocation density is much lower and the dislocations are less mobile. Interestingly, high-density SFs and twins have been observed in some ceramics, such as ZnS with low SFE (6 mJ/m^2) synthesized using vacuum hot-pressing technique (Fig. 1h) [79]. Recently, flash sintering has enabled the fabrication of fully dense ceramics with high-density defects [80–84]. Fig. 1i shows high-density dislocations and SFs in the flash-sintered TiO_2 [80]. Rapid sintering introduces plastic deformation at high temperatures within a short time followed by a rapid cooling process, which may generate and "freeze" a large number of dislocations and SFs in the flash-sintered TiO_2. Massive formation and migration of O vacancies occurring due to the electric field at the onset of flash sintering may also promote the creation of high-density defects after flash sintering [80].

3. SFs in FCC metals and their impact on mechanical behavior

Compared with the extensively studied TBs in FCC metals [1,9,10,13–15,38,44,45,85–99], there are scattered studies on the significant impact of SFs on the mechanical behavior of FCC metals. As mentioned previously, a recent study showed that a 1 μm thick metastable FCC Co film was stabilized with high-density SFs nucleating from the Cu/Co interface along multiple {111} planes (Fig. 1b) [56]. The mechanical behavior of the FCC Co film was tested using *in situ* pillar compression (Fig. 2) [56]. In general, the SFs in FCC Co contribute to hardening while maintaining good deformability. Surprisingly, both strain hardening and strain softening were observed in FCC Co with SFs depending on the applied strain rate. As shown in Fig. 2, considerable softening was observed in Co tested at low strain rate (1×10^{-3}/s), in contrast to the stress plateau at high strain rate (5×10^{-3}/s).

MD simulations revealed the deformation mechanisms of FCC Co nanopillar with pre-existing SFs [56]. Both strain hardening and softening were observed during compression. During the hardening stage, dislocation penetration is prohibited by intersecting SFs and the formation of Hirth locks (Fig. 3a1-a4). During the softening stage, partial dislocations cross slip along SFs, leading to defaulting and detwinning (Fig. 3b1-b4). The MD simulations, although performed at significantly higher strain rates than experiments, provide a plausible explanation for the strain-rate dependence. At low strain rate strain softening prevails due to insufficient density of Hirth locks. Whereas at higher strain rate, abundant Hirth locks form and can effectively resist the migration of partials, and lead to substantial work hardening. FCC single crystal metals with submicron pillar size often exhibit serrated flow behavior during plastic deformation [100–104] due to dislocation avalanches. However, in single crystal FCC Co, the inclined SF ribbons form barriers to the transmission of partial dislocations and suppress dislocation avalanches, which can only be achieved previously by increasing pillar diameter in single crystal FCC metals [102,105]. When SFs interact with dislocations in FCC metals, they can also nucleate new dislocations, which penetrate SFs or migrate along SFs. The latter mechanism has also observed analogously in TB-dislocation interactions, which improve the ductility of nanotwinned metals.

The interaction mechanisms between a screw dislocation and a single SF in FCC metals was studied via MD simulations by Wei et al. [106]. They showed that leading partial dislocations are generally blocked by the SF until recombination of the leading partial and the trailing partial occurs under sufficient external stress. The interactions between lattice screw dislocations and SFs are classified into three categories. First, a lattice dislocation dissociates into a partial dislocation and cross slips along the SF, forming an extrinsic SF (Fig. 3d). Second, a lattice dislocation dissociates into a partial dislocation and cross slips along the SF, leading to SF annihilation (Fig. 3e). Third, a lattice dislocation penetrates through the SF (Fig. 3f). The interaction is determined by various parameters including SFE, unstable SFE, and the applied shear stress. The stress necessary for the dislocation to cross slip along the SF or penetrate through the SF is higher than the critical resolved shear stress for the recombination of partial dislocations, leading to the strengthening effect of SFs [106].

To summarize, SFs in FCC metals play a valuable role in mitigating the strength-ductility trade-off. Strengthening by SFs depends on dislocation-SF interactions as well as SF configuration, while plastic deformation is accommodated by cross-slip of partial dislocations along SFs.

4. SFs in HCP metals and their role in mechanical behavior

Although FCC metals with SFs have been less well investigated, there

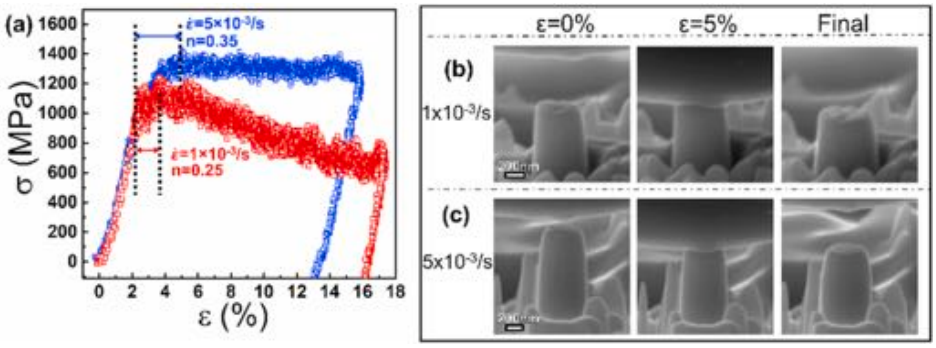

Fig. 2. *In situ* SEM micropillar compression tests showing strain rate dependent deformation of FCC (100) Co [56]. (a) Strain softening was observed at low strain rate (1×10^{-3}/s, red), whereas prominent strain hardening was observed at a high strain rate (5×10^{-3}/s, blue). (b–c) *In situ* SEM snap shots show that the FCC (100) Co pillars exhibited prominent barreling. (For interpretation of the references to color in this figure legend, the reader is referred to the Web version of this article.)

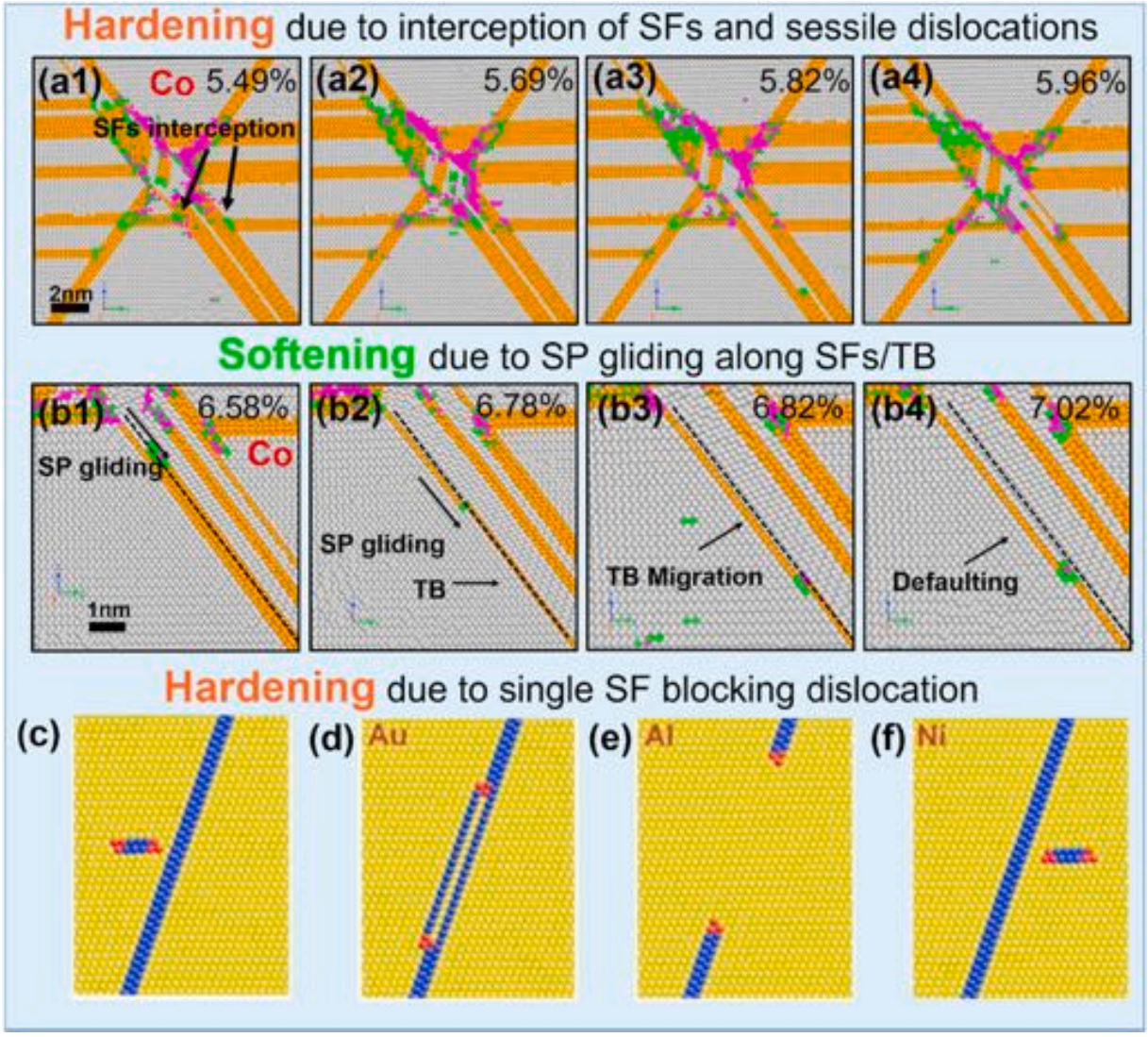

Fig. 3. (a,b) Atomistic simulation of deformation in FCC Co with intercepted SFs using common neighbor analysis [56]. (a1-a4) In the hardening region, the interception of SFs leads to sessile locks, and the thickening of SFs leads to the HCP Co. (b1-b4) At a higher strain level, a SF was initially blocked by an HCP laminate, then the Shockley partial from the SF glided along the HCP phase, leading to gradual defaulting and softening. (c) A screw dislocation approaches the SF and interactions are categorized as 3 modes [106]. (d) For the mode 1 in Au, after interaction, a SF envolved into an extrinsic SF by the emission of two twinning partials adjacent to the SF. (e) For the mode 2 in Al, after interaction, a SF was annihilated by the emission of two trailing partials along the SF. (f) For the mode 3 in Ni, lattice dislocation transmitted across the SF.

are scattered studies on deformation mechanisms of HCP metals with high-density SFs. Wu et al. prepared 2 μm nanocrystalline Ti films with abundant SFs as shown in Fig. 4a–d [59]. Nanoindentation tests show that the strength σ (Hardness/2.7) of nanocrystalline Ti with SFs can approach 4.4 GPa (Fig. 4e). Compared with strength of Ti in other studies, the nanocrystalline Ti with SFs has highest strength σ and largest Hall-Petch slope K_{SF}. The fundamental strengthening mechanisms remain unclear.

Jian et al. [63] fabricated Mg alloys with nanoscale SFs via hot rolling. With the increasing rolling strain, the average SF spacing decreased to 16 nm (Fig. 1d). Tensile tests (Fig. 5a) showed that the yield strength increased with reduction in thickness. The ductility of Mg alloys (Fig. 5) decreases after the initial 50% thickness reduction after hot rolling, but further increase in rolling strain leads to strengthening without additional deterioration of the ductility. Fig. 5b shows a linear relationship between yield strength and the reciprocal of the average SF spacing, $1/d$. It is worth mentioning that this linear relationship has only been observed in HCP Mg, and further investigations are necessary in other materials with nanoscale SFs. Post deformation TEM analyses show that some SFs were broken into short segments (Fig. 5c), and high-density dislocations were trapped in between SFs (Fig. 5d). These observations indicate that dislocations slip along pyramidal or prismatic planes are blocked by SFs, which lead to strengthening. The accumulation of dislocations between SFs enables work hardening capability.

Su et al. [54] sputter-deposited HCP Co with high-density parallel SFs on basal planes (Fig. 1c). *In situ* micropillar compression tests showed that HCP Co with SFs had a high yield strength, 1.1 GPa and work hardened significantly to a flow stress of 2.0 GPa (Fig. 6a). SEM snapshots during compression (Fig. 6b–e) show that HCP Co experiences a uniform deformation without forming any cracks or shear bands up to 20% strain. Post deformation TEM analyses (Fig. 7) reveal that FCC Co phase formed after compression and high-density inclined SFs in FCC phase were observed (Fig. 7c and d). This observation suggests that HCP–to-FCC phase transformation dominates the plasticity in HCP Co since dislocation slip and deformation twinning are prohibited due to crystal orientation, parallel SFs and small columnar grain size [54]. MD simulations (Fig. 8) probed the atomistic deformation mechanisms and detailed phase transformation process of HCP Co pillars with SFs. As the

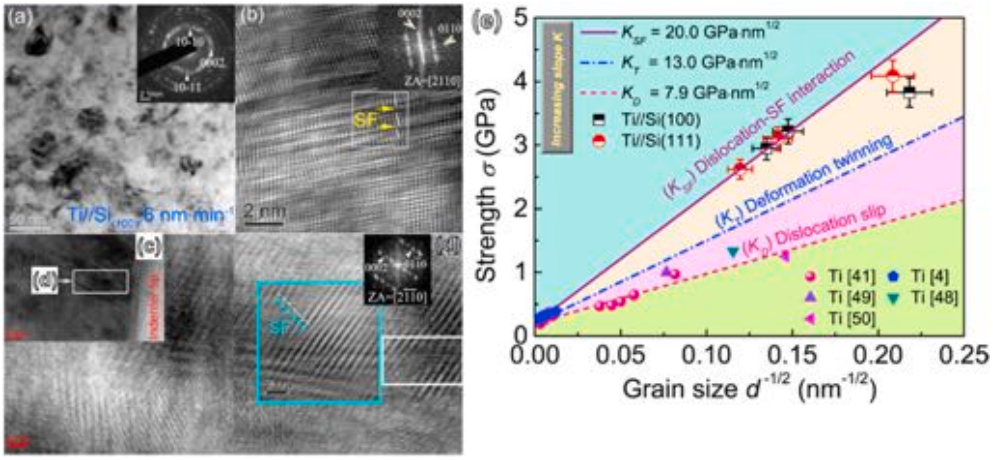

Fig. 4. (a,b) TEM and HRTEM images of Ti film samples showing SFs before deformation. (d) is the magnified view of the boxed regions in (c) near to the indenter tip, showing the SF-dislocation interactions. (e) The strength vs. grain size plot shows a greater Hall-Petch slope of $K_{SF} = 20.0$ GPa nm$^{1/2}$ for SF strengthening than those of deformation twinning and dislocation slip [59].

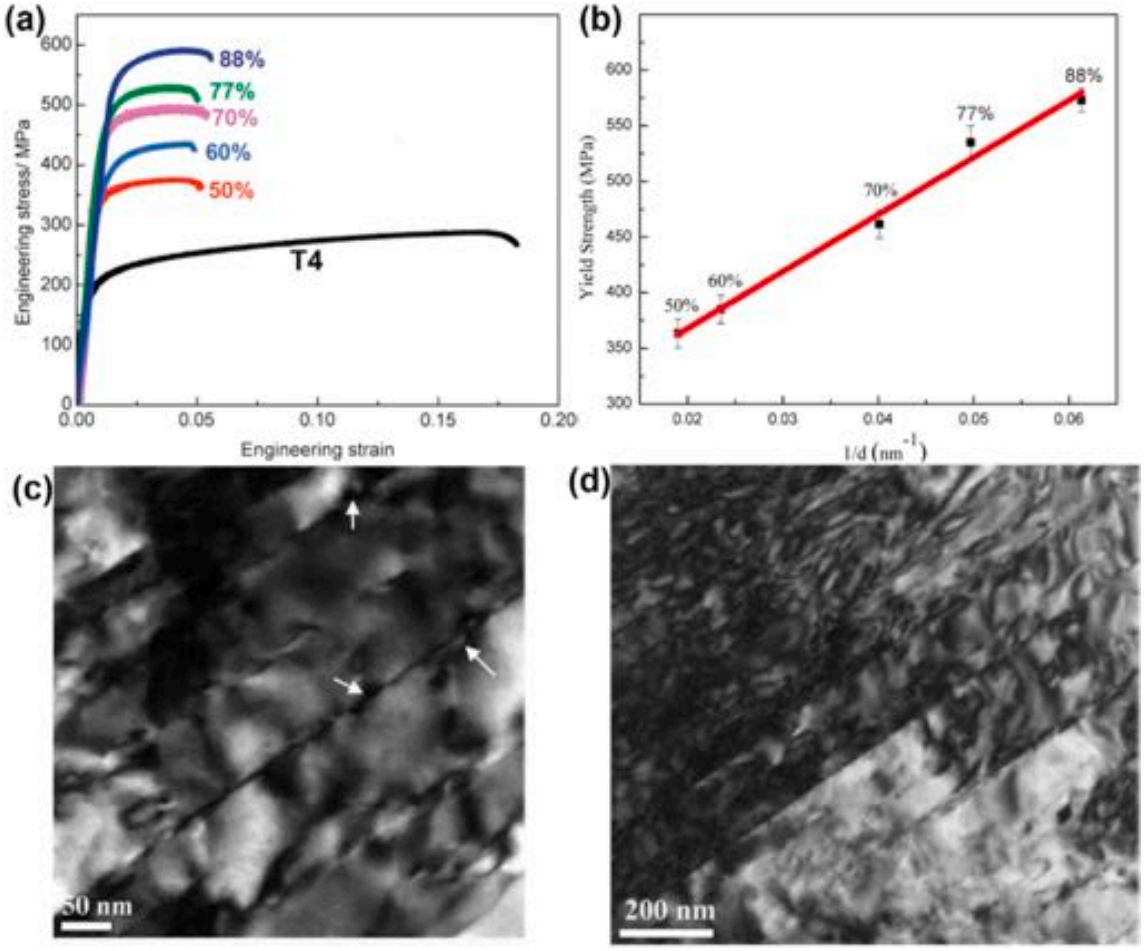

Fig. 5. (a) Engineering stress–strain curves of Mg alloys [63] after hot rolling with different thickness reductions. (b) Yield strength increases monotonically with the reciprocal of SFs spacing of the hot rolled Mg alloys. (c) TEM images of 88% hot rolled Mg alloy after tensile test showing SFs interacted with dislocations marked by white arrows. (d) High-density -dislocations were observed between SFs.

stress increases, Shockley partials start to glide along the SF planes, resulting in defaulting (Fig. 8c). The increase of SF spacing facilitates the nucleation of FCC Co phase on the inclined {111} planes (Fig. 8d). The glide of Shockley partials in the FCC Co phase on the inclined (111) planes leads to SFs (HCP Co) in the FCC phase, and triggers plastic yielding manifested by a major stress drop (Fig. 8a). Phase transformation generally requires higher stress, thus strengthens the pillar, while it also accommodates plastic deformation.

In summary, SFs enhance the mechanical strength of HCP metals by hindering dislocation migration, similar to the strengthening

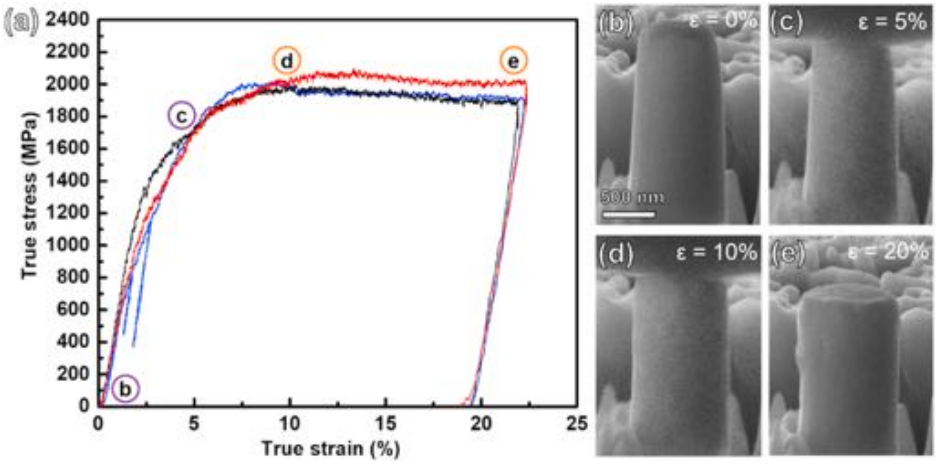

Fig. 6. *In situ* micropillar compression tests on HCP Co at a strain rate of 5×10^{-3}/s [54]. (a) True stress-strain curves show HCP Co has prominent work hardening and a flow stress approaching 2 GPa. (b–e) SEM snapshots of an HCP Co pillar showing uniform deformation.

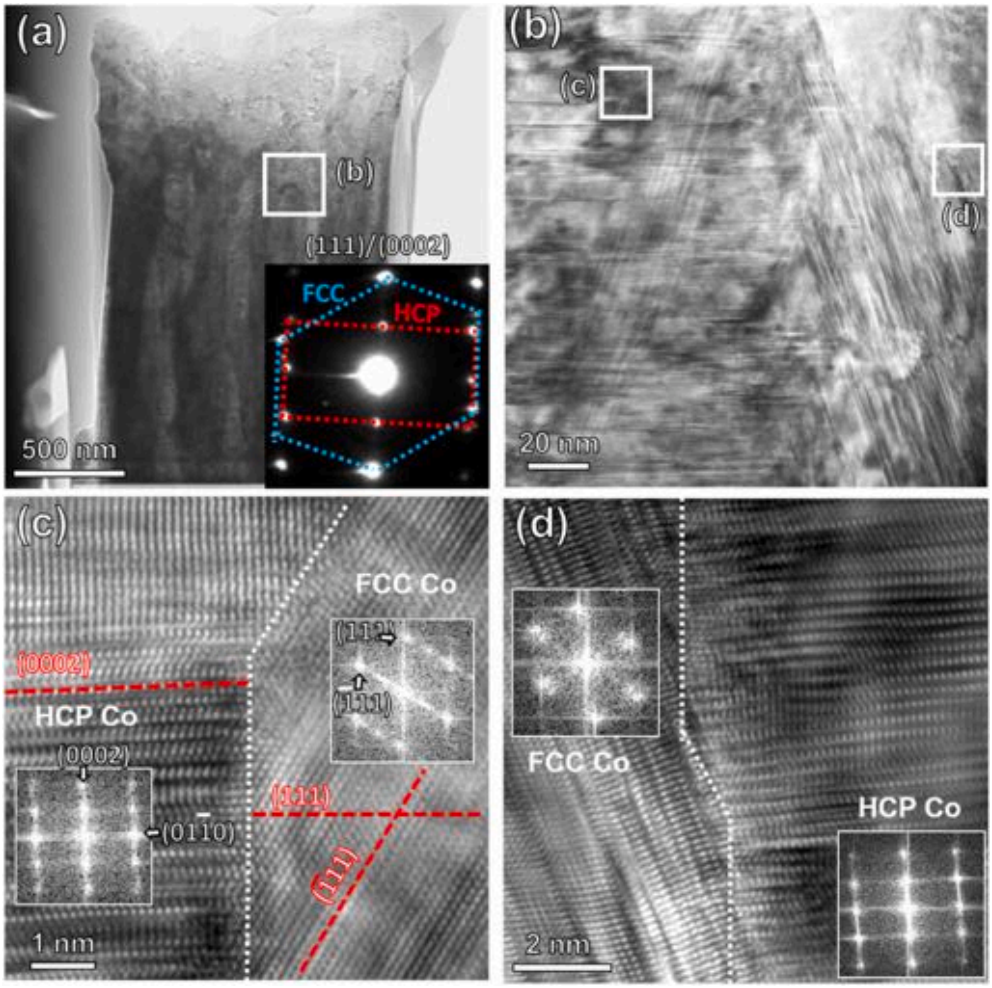

Fig. 7. Cross-section TEM micrographs of a HCP Co pillar deformed to 20% true strain [54]. (a) A low magnification TEM micrograph showing no shear bands or cracks. (b) A higher magnification TEM micrograph shows inclined SFs (c, d) HRTEM micrographs of the boxes in Fig. 7b show the coexistence of FCC and HCP Co. High-density inclined SFs were captured in FCC Co.

mechanism observed in FCC metals. In addition, if dislocations glide along SFs, HCP-to-FCC phase transformation is triggered to accommodate plasticity, especially when dislocation and deformation twinning are inhibited in nanoscale samples. Thus, SFs in HCP metals are effective to simultaneously strengthen the material and accommodate plasticity.

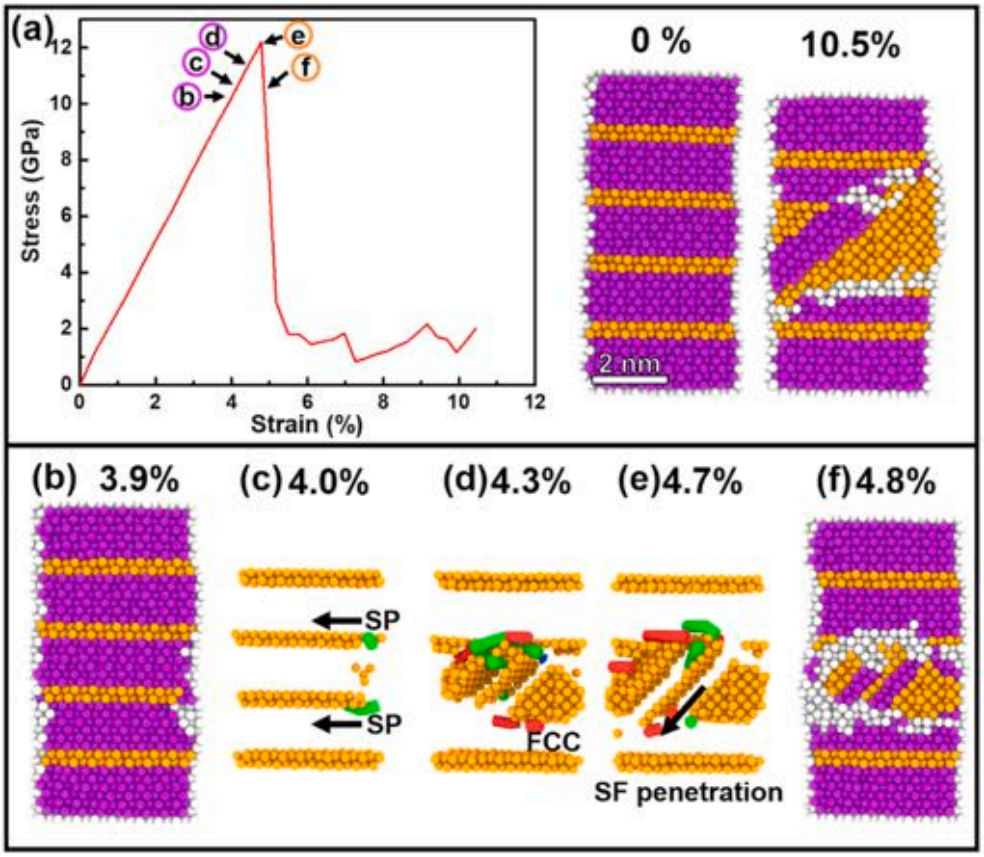

Fig. 8. MD simulations of compression tests of HCP Co pillar with parallel SFs [54]. Orange, purple and white colors correspond to FCC, HCP and unidentified structures, respectively. Green and red lines are Shockley partial dislocation and other dislocations including stair rod dislocations. (a) Left panel: The stress-strain curve shows a high yield strength of 12 GPa. Right panel: HCP Co pillar before and after compression (to 9.8% strain). HCP-to-FCC phase transformation was observed. (b) Elastic deformation in the HCP Co pillar to a strain of 3.9%. (c) When $\varepsilon = 4.0\%$, Shockley partials emerge along SF planes. (d) When $\varepsilon = 4.3\%$, the Shockley partials glide along SFs, causing defaulting of the pre-existing SFs and of FCC Co forms on the inclined planes. (e) At 4.7%, inclined SFs form in FCC Co and penetrate through the preexisting horizontal SFs, leading to the stress drop. (f) By 4.8%, the density of inclined SFs increases while some of the horizontal SFs are removed. (For interpretation of the references to color in this figure legend, the reader is referred to the Web version of this article.)

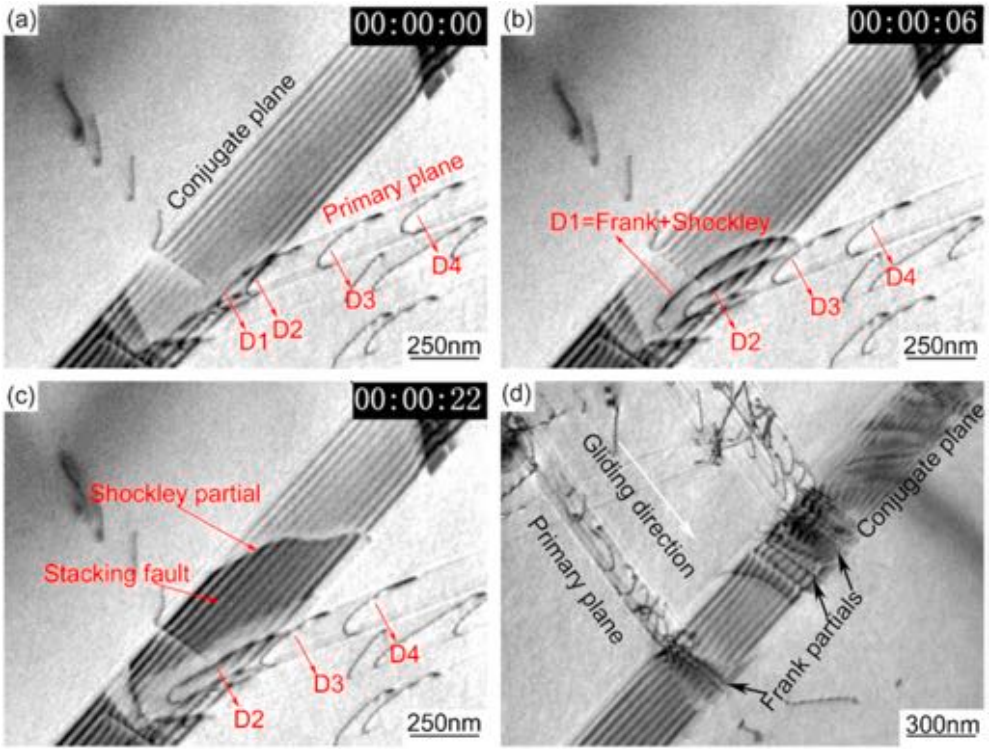

Fig. 9. *In situ* TEM study showing dislocation-SF interactions in $FeCoNiCrAl_{0.1}$ high entropy alloy [75]. (a–b) TEM images showing the cross slip of the dislocations from the primary plane to the conjugate plane. (c) TEM images of the cross-slip dislocation dissociated into a Frank and Shockley partial. A SF formed via partial migration. (d) Frank partials formed on the conjugate planes.

5. SFs in high entropy alloys and their roles in mechanical behavior

High entropy alloys have received broad attention due to their unique microstructure and properties [58,60,64,72–77,107–115]. Traditional alloys are usually based on one primary element, with additional elements added to tune the microstructure and the resulting properties. However, high entropy alloys normally contain several elements with similar concentration, forming simple crystal structures, such as FCC or BCC structure, thus producing a stable solid solution state and high entropy of mixing [77,111–113,115]. Interestingly, in some FCC high entropy alloys with low SFE, SFs have been observed and these defects can largely impact the deformation mechanisms and mechanical properties. In this section, we will discuss the role of SFs in these high entropy alloys in tailoring mechanical properties.

Bulk $FeCoNiCrAl_{0.1}$ system with their low SFE, ~30 mJ/m^2, was studied by Liu et al. [75] using *in situ* technique to investigate the twinning behavior during plastic deformation. Dislocations that slip along the primary slip planes were blocked by the SF ribbon (Fig. 9), showing similar strengthening effect of SFs by impeding dislocation motion. Cross-slip along the conjugate plane was also observed, leaving behind a Frank dislocation on the SF. This study demonstrates that cross-slip is important to twin nucleation and thickening, induced by partial dislocation migration along SFs and TBs. Thus, SFs in $FeCoNiCrAl_{0.1}$ effectively block dislocations migration and promote twinning.

The microstructure and mechanical properties of $Al_{0.1}CoCrFeNi$ thin films prepared via sputtering were investigated by Feng et al. [58]. At a greater deposition rate, the $Al_{0.1}CoCrFeNi$ alloy has more SFs, denoted as SF $Al_{0.1}CoCrFeNi$ (Fig. 10a and b), whereas more growth twins were observed in the specimen at lower deposition rate (denoted as NT $Al_{0.1}CoCrFeNi$ shown in Fig. 10c and d). Micropillar compression tests (Fig. 10e and f) show intrinsic and extrinsic size effects. The power law exponent of SF $Al_{0.1}CoCrFeNi$ is greater than that of NT $Al_{0.1}CoCrFeNi$, indicating a greater work hardening ability. Also the flow stresses of SF $Al_{0.1}CoCrFeNi$ is slightly greater than that of NT $Al_{0.1}CoCrFeNi$ (Fig. 10g). Furthermore, the SF $Al_{0.1}CoCrFeNi$ pillar has better deformability than the NT $Al_{0.1}CoCrFeNi$ (Fig. 10h and i). The authors suggested that SFs were more stable than TBs at the nanoscale, while detwinning was frequently observed when twin spacing is several nm [45,116].

SFs were also observed in the FCC phase in dual-phase high entropy alloys [60,64,117,118]. By tuning the Mn concentration, Li et al. prepared $Fe_{50}Mn_{30}Co_{10}Cr_{10}$ with low SFE and reported its superior mechanical properties (Fig. 11a) [60]. A large number of SFs were observed in the FCC matrix and HCP laminates (Fig. 11b and c). During early stages of plastic deformation, contrary to the HCP-to-FCC phase transformation observed in HCP metals discussed earlier [54], stress induced the FCC-to-HCP phase transformation in $Fe_{50}Mn_{30}Co_{10}Cr_{10}$. The phase transformation induced plasticity together with dislocations contributes to the good ductility of the dual phase $Fe_{50}Mn_{30}Co_{10}Cr_{10}$. Moreover, the FCC/HCP phase boundaries acted as obstacles to dislocation migration and contributed to strain hardening. During the later stage of the plastic deformation, deformation induced nanotwins and SFs formed continuously in the HCP phase, and significantly strengthened the material.

To summarize, SFs are generally observed in the FCC phase of high entropy alloys with low SFE, and can effectively strengthen the alloys by impeding dislocation migration. Meanwhile, SFs are critical in maintaining plasticity of high entropy alloys by allowing cross-slip and promoting FCC-to-HCP phase transformations.

6. SFs in ceramics and their role in mechanical behavior

Ceramics have many advantages over metallic materials including high hardness, superior wear and corrosion resistance, and high temperature stability [80,81,119–126]. However, applications of ceramics have been limited due to their poor ductility at low temperature. This brittleness at room temperature is attributed to the lack of dislocations owing to the ionic or covalent bonding in ceramics. One of the approaches to improve room temperature plasticity of ceramics is to introduce preexisting planar defects including TBs and SFs [80–82,119,127,128].

A recently developed sintering technique, known as flash-sintering, can sinter ceramics to full density within several seconds [80–84,119,127–138]. Li et al. [80] fabricated TiO_2 using flash-sintering and observed high-density preexisting SFs (Fig. 1i). SFs can be created due to the formation of oxygen non-stoichiometry during flash sintering. An external electric field can generate electrochemically reducing environment for TiO_2 thereby producing a high density of oxygen vacancy [139]. Consequently, SFs can be formed by coalescence of the

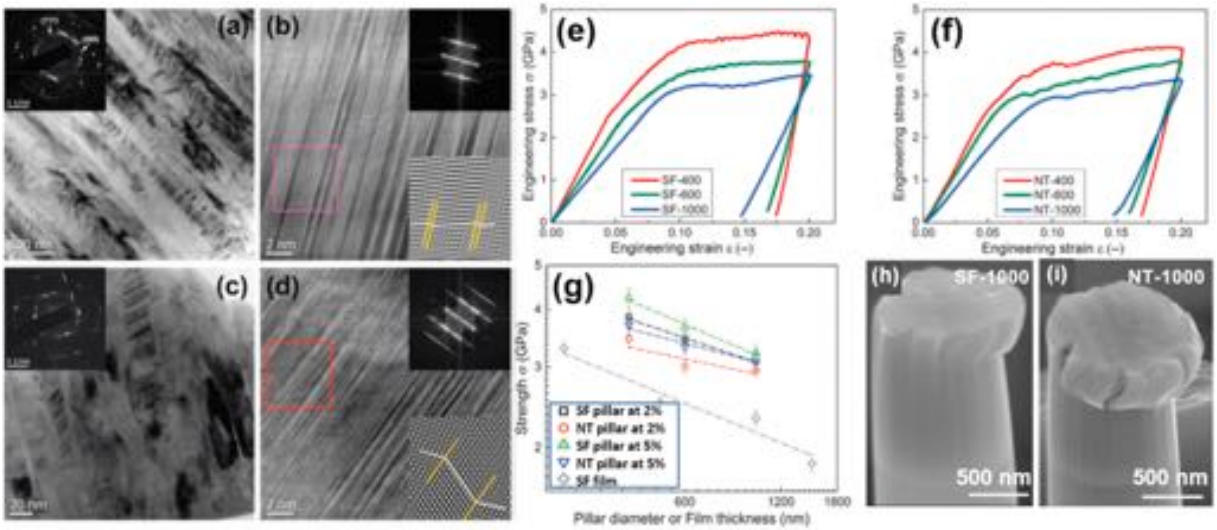

Fig. 10. (a–d) Microstructures of the $Al_{0.1}CoCrFeNi$ high entropy alloy with SFs and nanotwins sputter-deposited at high and low deposition rates. (a–b) TEM images show columnar grains with SFs in (111) textured films. (c–d) The TEM images of $Al_{0.1}CoCrFeNi$ with numerous nanotwins. (e–f) Compression engineering stress–strain plots of alloy pillars with SFs or nanotwins measured at room temperature. The pillars have different diameters (400, 600 and 1000 nm). (g) Comparison of the strength of SF and NT (nanotwinned) high entropy alloy pillars at different strains (2% and 5%) as a function of pillar diameter or film thickness. (h–i) Deformed pillars with SFs or nanotwins with a diameter of 1000 nm [58].

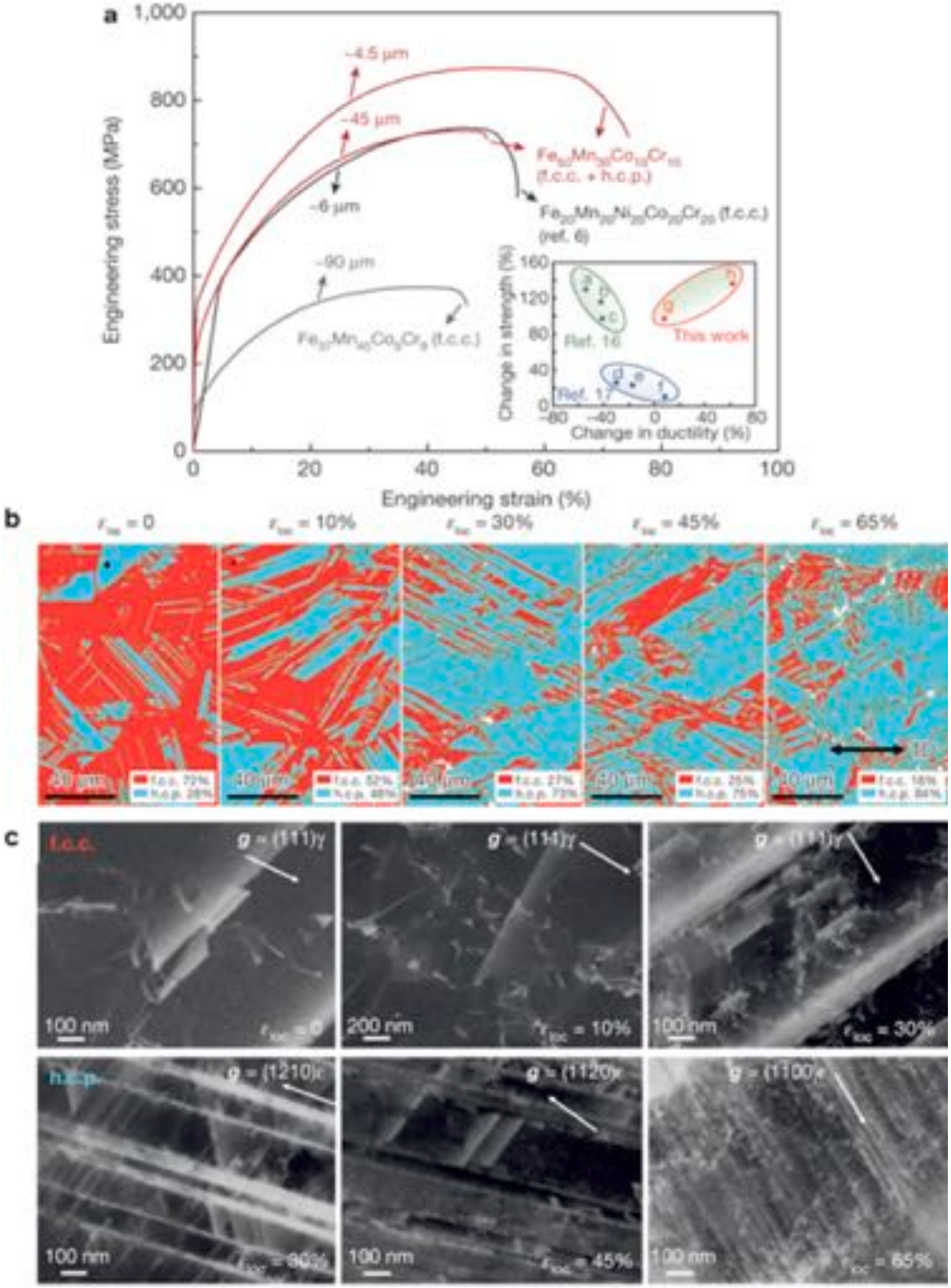

Fig. 11. (a) Mechanical behavior of the TRIP dual phase high entropy alloys (red curves) compared to various single-phase high entropy alloys. (b) EBSD phase maps showing the evolution of deformation-induced martensite at various local strain, $\varepsilon_{loc.}$ TD is the tensile direction. (c) Electron channeling contrast imaging analyses showing the evolution of microstructures in the FCC and HCP phases. γ is the FCC phase and ε is the HCP phase [60]. (For interpretation of the references to color in this figure legend, the reader is referred to the Web version of this article.)

high-density oxygen vacancies into planar faults [140]. Conventional TiO_2 exhibits catastrophic brittle failure at ~2% strain at room temperature (Fig. 12A1-6). Flash-sintered TiO_2 shows prominent work hardening ability to a flow stress of 2–2.5 GPa and small serrations on the stress-strain curves implying much better plasticity at room temperature than the conventional TiO_2. Post deformation TEM images show high-density SFs formed along shear band direction (Fig. 12c1,2), with minor SFs along different direction (Fig. 12c3). O vacancies and preexisting SFs promote defect nucleation and propagation during plastic deformation. Thus, plastic deformation can be accommodated by propagation of SFs and work hardening capability is improved due to high defect density.

SFs have also been observed in ZnS due to its low SFE, ~ 6 mJ/m^2 [79,141,142]. Cho et al. [79] investigated the mechanical properties of ZnS prepared by vacuum hot-pressing technique. TEM images of as-sintered ZnS in Fig. 1h (left) reveal the high-density TBs and SFs in a sphalerite phase. *In situ* micropillar compression tests were conducted on the pillars with a diameter of 3 μm at a constant strain rate of 5×10^{-3}/s at room temperature as shown in Fig. 13a–e. The 3 μm pillars fractured at different stress and strain levels due to the brittle nature of ZnS, but still exhibited certain strain-hardening capability, in a drastic contrast to many brittle semiconductors and ceramics tested at room temperature. The strain hardening capability may arise from the hinderance of migration of Shockley partials by preexisting SFs and TBs shown in (Fig. 13f–h) [79].

In summary, preexisting SFs can prominently increase the room temperature plasticity of ceramics via promoting dislocation nucleation during deformation and enhancing work hardening capability. It is worth emphasizing that although there are scattered experimental studies on ceramics with SFs, computational investigations on the SF-mediated deformation mechanisms in ceramics remain scarce.

7. SFs in metallic multilayers and their role in mechanical behavior

Some metallic multilayers have shown SFs coexisting with other planar defects including TBs and layer interfaces. Zhang et al. studied the mechanical behavior of Al/Ti multilayers [3] with high density SFs (Fig. 14). TEM analyses confirm that the volume fraction of SFs increases with decreasing layer thickness and reaches a maximum of ~ 40% when layer thickness is 2 nm (Fig. 14f). These high-density SFs may nucleate from Al/Ti layer interfaces to reduce the strain energy of the multilayers. As shown in the Hall-Petch plot in Fig. 14g, hardness plateau or softening typically occurs when $h < 10$ nm. The softening often derives from

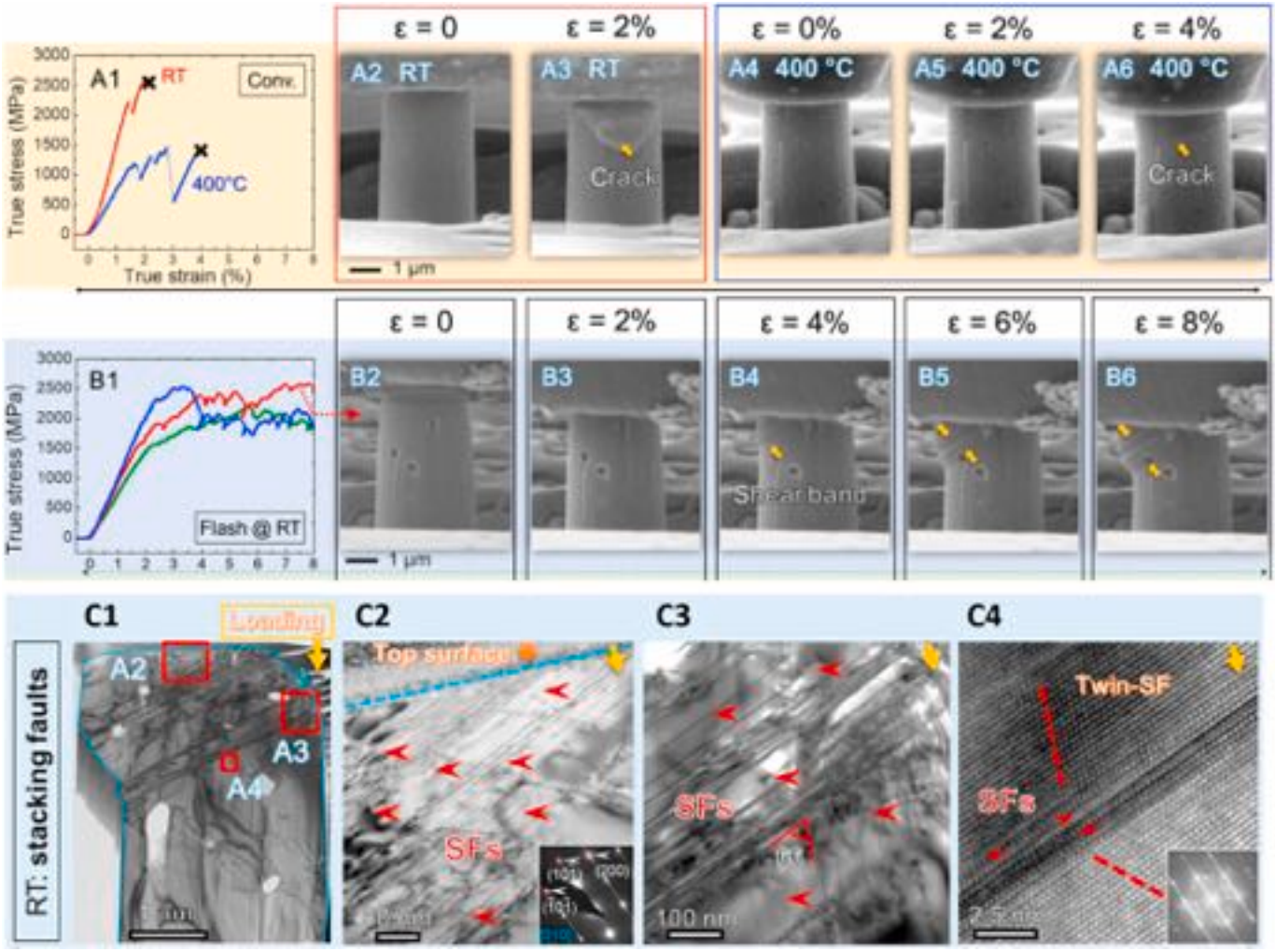

Fig. 12. *In situ* microcompression tests on the conventional and flash-sintered TiO_2 at room temperature (RT) and 400 °C, at a constant strain rate of 5×10^{-3} s^{-1} [80]. (A1 to A6) Representative stress-strain curves and SEM snap shots of conventional sintered TiO_2 pillars showing brittle fractures at an average true strain of 2-3%, and 400 °C. (B1 to B6) Flash-sintered TiO_2 tested at RT showing work hardening to a flow stress of beyond 2 GPa. The *in situ* SEM snapshots show successive high-density slip bands. Fracture was absent up to a strain of 8%. (C1-C4) TEM micrographs of flash-sintered TiO_2 pillars after compression tests at room temperatures showing the deformation induced straight shear bands consist of abundant SFs and TBs.

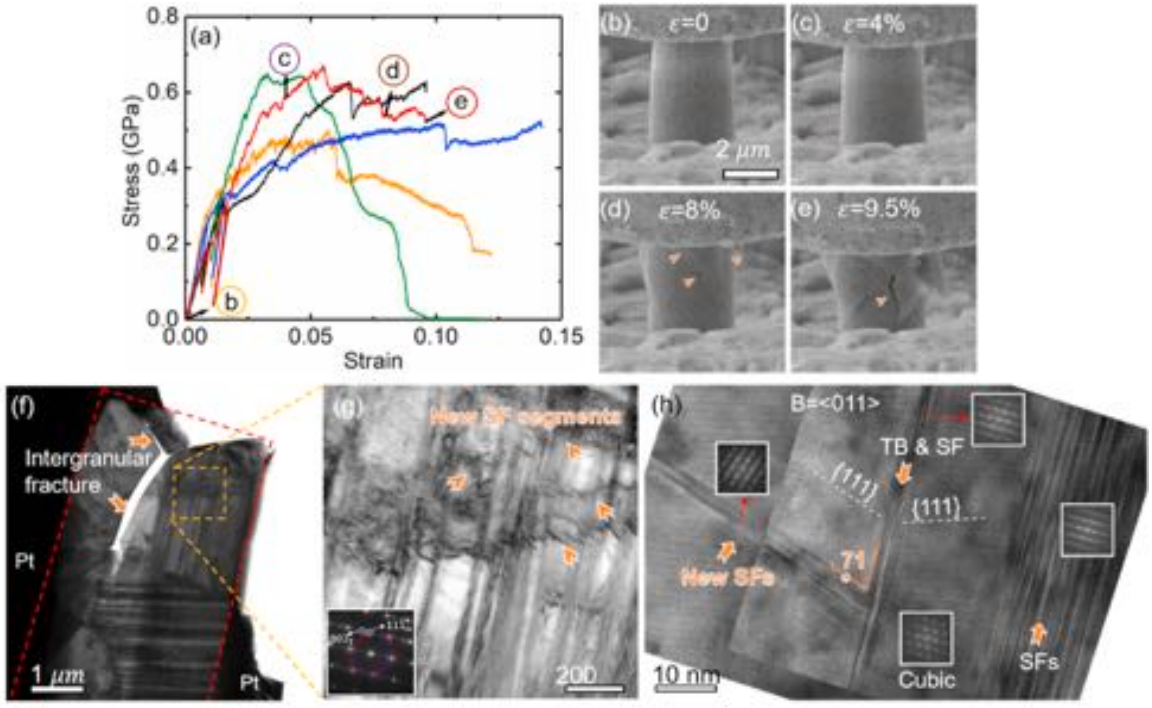

Fig. 13. *In situ* compression studies of ZnS micropillars with a diameter of 3 μm at a constant strain rate of 5×10^{-3}/s at room temperature [79]. (a) The stress-strain curves show moderate strain hardening capability of ZnS. (b–e) SEM snapshots of the pillar corresponding red stress-strain curve showing that noticeable cracks at 8% strain. (f) TEM image shows evident intergranular crack and high-density SFs and TBs. (g) Pre-existing SFs deformation induced short SFs indicated by orange arrows. Inserted SAD pattern shows the presence of SFs and TBs. (h) HRTEM image shows that the deformation induced SF segment was blocked by pre-existing TBs and SFs. (For interpretation of the references to color in this figure legend, the reader is referred to the Web version of this article.)

coherent layer interface, a weak barrier to dislocation transmissions, or the substantial decrease in Koehler stress due to the spread of dislocation cores across several layers [3]. In comparison, no softening has been identified in the Al/Ti multilayer, and the hardness of multilayers increases to 7.4 GPa when $h = 1$ nm. They ascribe the absence of softening to the formation of the high-density SFs, which can generate slip discontinuity and introduce extra strengthening in the Al/Ti multilayers. Also, a recent study by the same authors demonstrates that SFs can enhance the deformability and work hardening capability of Al/Ti multilayers by facilitating the glide of partial dislocations [143].

Su et al. [55] recently studied the mechanical behavior of Cu/Co multilayers. They reported that Cu (111)/Co (0002) 25 nm multilayers have defect networks containing high-density TBs in the Cu layers, SFs in the Co layers and incoherent layer interfaces (Fig. 15a–e). The yield strength of the Cu/Co 25 nm multilayer is 2.4 GPa and its flow stress exceeds 3 GPa, much greater than many ductile multilayer systems (Fig. 15f) [144–150]. The Cu/Co 25 nm multilayer with these defect networks also exhibits good plasticity under compression (Fig. 15g). Post-deformation TEM study shows that TBs and SFs are effective in blocking partial migration. In addition, the SFs in HCP Co layers promote HCP-to-FCC phase transformation (Fig. 15h and i), and the deformation mechanism is similar to that of single crystal HCP Co with SFs. MD simulations (Fig. 16) reveal a collaborative strengthening mechanism enabled by TBs, SFs and incoherent interfaces. Before yielding, TBs can effectively block partial migration until detwinning occurs (Fig. 16d). Partial migration is also prohibited by SFs and incoherent interfaces. Yielding starts when HCP-to-FCC phase transformation occurs in Co layers (Fig. 16e). As a consequence, incoherent FCC Cu/HCP Co interfaces transform into coherent FCC Cu/FCC Co interfaces, and partial dislocation can now easily migrate through the layer interface (Fig. 16f). Thus, in this defect network enabled strengthening mechanism, SFs strengthen the multilayers by blocking dislocations and enhance plasticity by promoting phase transformation.

8. Summary of the impact of SFs on mechanical behaviors and outlook

Similar to other planar defects including GBs, TBs and layer interfaces, the impact of SFs on mechanical behavior is closely related to dislocation-SF interactions. In what follows, we summarize some overarching features related to dislocation-SF interactions and elucidate their atomistic underpinnings.

When dislocations slip along planes inclined to SFs, SFs (often in form of SF ribbons) serve as effective barriers to dislocation migration, similar to TB-dislocations and GB-dislocation interactions. After the SF intercepts a dislocation, the SF is either broken into discontinuous smaller segments [63,79,106] or absorbs the incoming dislocation and nucleates a new dislocation that could penetrate through the SF or could cross slip along the SF [56]. Both mechanisms require higher stress and thus contribute to strengthening (Fig. 17a–f). In FCC structures, SFs on different {111} planes intercept and form Lomer Cottrell Locks or Hirth Locks at the SF interceptions (Fig. 17g-l) [55,56,79]. These sessile dislocations are stable during deformation and inhibit partial dislocation migration along both inclined and parallel {111} planes, and thus greatly strengthen materials. Meanwhile, the strengthening effect is closely related to the density of SF interceptions and sessile dislocations.

Two key mechanisms exist for SFs improved plastic deformation. First, a dislocation gliding along a SF induces a defaulting process that leads to softening and sustained plasticity (Fig. 18a–f). This phenomenon was observed in FCC Co at lower strain rate when the density of Hirth locks and SFs intersections is low [56] (Fig. 18e and f). When dislocations continue to glide along the SFs in the same direction, shear bands form [55,80]. Second, when partial dislocations glide along SFs, they alter the stacking sequence and promote phase transformations between the HCP and FCC phase (Fig. 18g–i) [54,55,60,72,143]. It has been shown that phase transformation can greatly enhance the plasticity in multilayers [54,55,143] and high entropy alloys [60,64,72] via

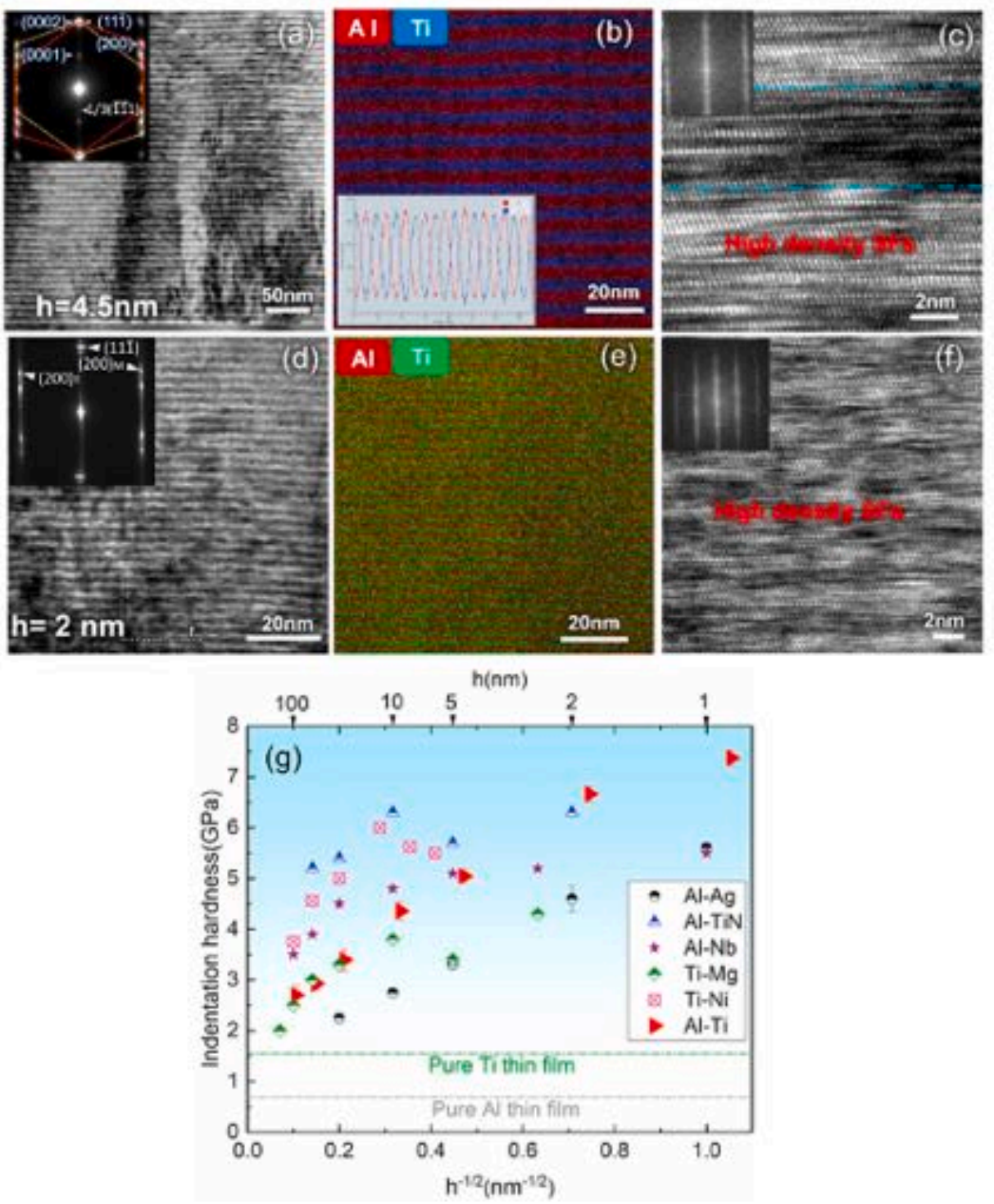

Fig. 14. XTEM micrograph of Al/Ti 4.5 nm multilayer (a–c) and Al/Ti 2 nm multilayer (d–f) [3]. (a) Overview XTEM micrograph and SAD pattern showing the FCC twinned Al and HCP Ti. (b) EDS map and composition line scan showing clear Al/Ti layer interfaces. (c) HRTEM image showing the coexistence of FCC and HCP Ti. (d) XTEM image and SAD pattern showing the twinned FCC Al and Ti layer. (e) EDS map showing alternatinglayer structures. (f) HRTEM micrograph of high-density SFs in Al and Ti. (g) Comparison of indentation hardnessvs. $h^{-1/2}$ (h is the average layer thickness) for Al or Ti based multilayer systems.

alignment of the crystal lattice along the preferential direction and offering of additional slip systems.

In Conclusion, SFs are promising planar defects observed in a variety of metallic materials and can improve strengthening and plasticity simultaneously. Furthermore, SFs promote partial migrations and phase transformations, and thus offer opportunity for improving ductility.

We have shown that both TBs and SFs are effective in blocking the propagation of dislocations, thus inducing significant strengthening and work hardening in materials [7,8,11,15–19]. However, SFs seem to introduce intriguing strain rate sensitivity in metallic materials. Strain hardening is observed at high strain rate, whereas strain softening prevails at low strain rate in FCC Co. Such an intriguing phenomenon has not been observed in nanotwinned metals. Also, as mentioned earlier, the interaction of dislocations with TBs may lead to detwinning, whereas

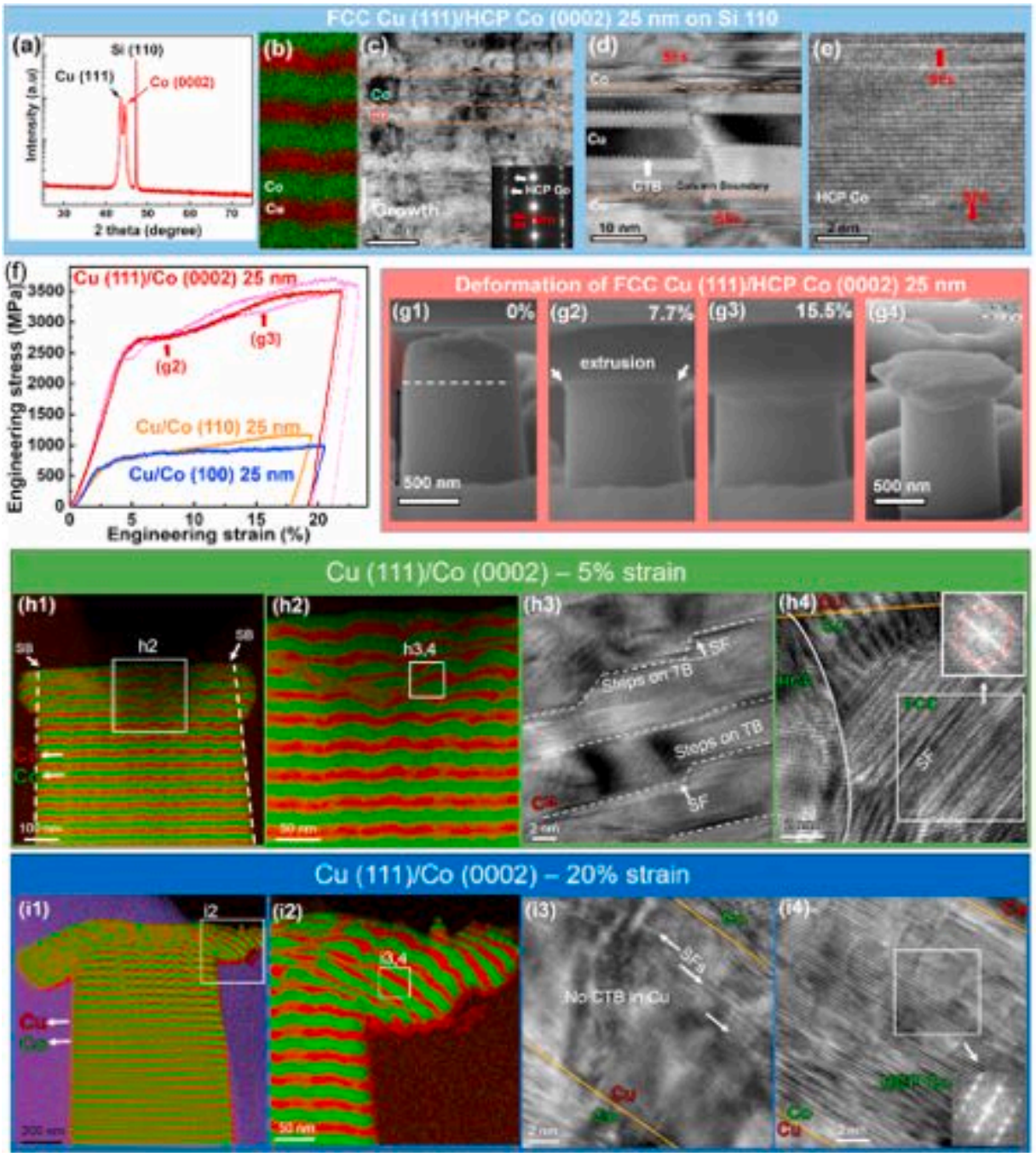

Fig. 15. (a) XRD profile showing the highly textured Cu (111)/Co (0002) 25 nm multilayer film on Si (110) substrate [55]. (b–e) XTEM micrographs showing the defect networks containing incoherent layer interfaces, SFs in HCP Co and CTBs in Cu. (f) Engineering stress-strain curves show that Cu (111)/Co (0002) pillars have much higher yield strength, ~2400 MPa than the (110) and (100) textured FCC Cu/Co 25 nm speimens. (g1-g4) SEM images of the Cu (111)/Co (0002) 25 nm multilayer show significant plastic deformation near the top of the pillar manifested as a cap. (h1-h2) EDS maps of the Cu (111)/Co (0002) 25 nm pillar deformed to 5% true strain showing deformation of the pillar top. (h3) Defective TB containing steps in the Cu layers. (h4) FCC Co phase with inclined SFs formed near the Cu/Co interface as confirmed by the inserted FFT. (i1-i2) EDS map of the multilayer deformed to 20% strain showing significant expansion of the pillar top. (i3, i4) HRTEM micrographs of the pillar top show detwinning in the Cu layer, and high-density SFs in the HCP Co layer.

the cross-slip of partials along SFs may lead to defaulting or the formation of TBs [11]. Comparing to the investigations on TB induced strengthening and plasticity, the studies on SFs dominated deformation mechanisms require significant attentions. First, the general impact of SFs on mechanical behavior of materials have been reported in several metallic and ceramic materials. More studies are necessary to substantiate the mechanisms for the formation and evolution of SFs before and during deformation. Second, the thermal stability of SFs and the influence of SFs on high temperature mechanical behavior of materials remain unclear. Third, the size effect on SF dominated deformation mechanisms should be investigated further. Fourth, there is a need to compare and distinguish the role of SFs and TBs on deformation mechanisms in materials. Quantitative studies on the difference in stress barriers posed by various planar defects (SFs, TBs and GBs) are desirable. Finally, the influence of SFs on the physical properties of materials is less well understood. For instance, the role of SFs on electrical conductivity and magnetic properties of materials requires further investigations. Recently TBs have shown to largely improve radiation

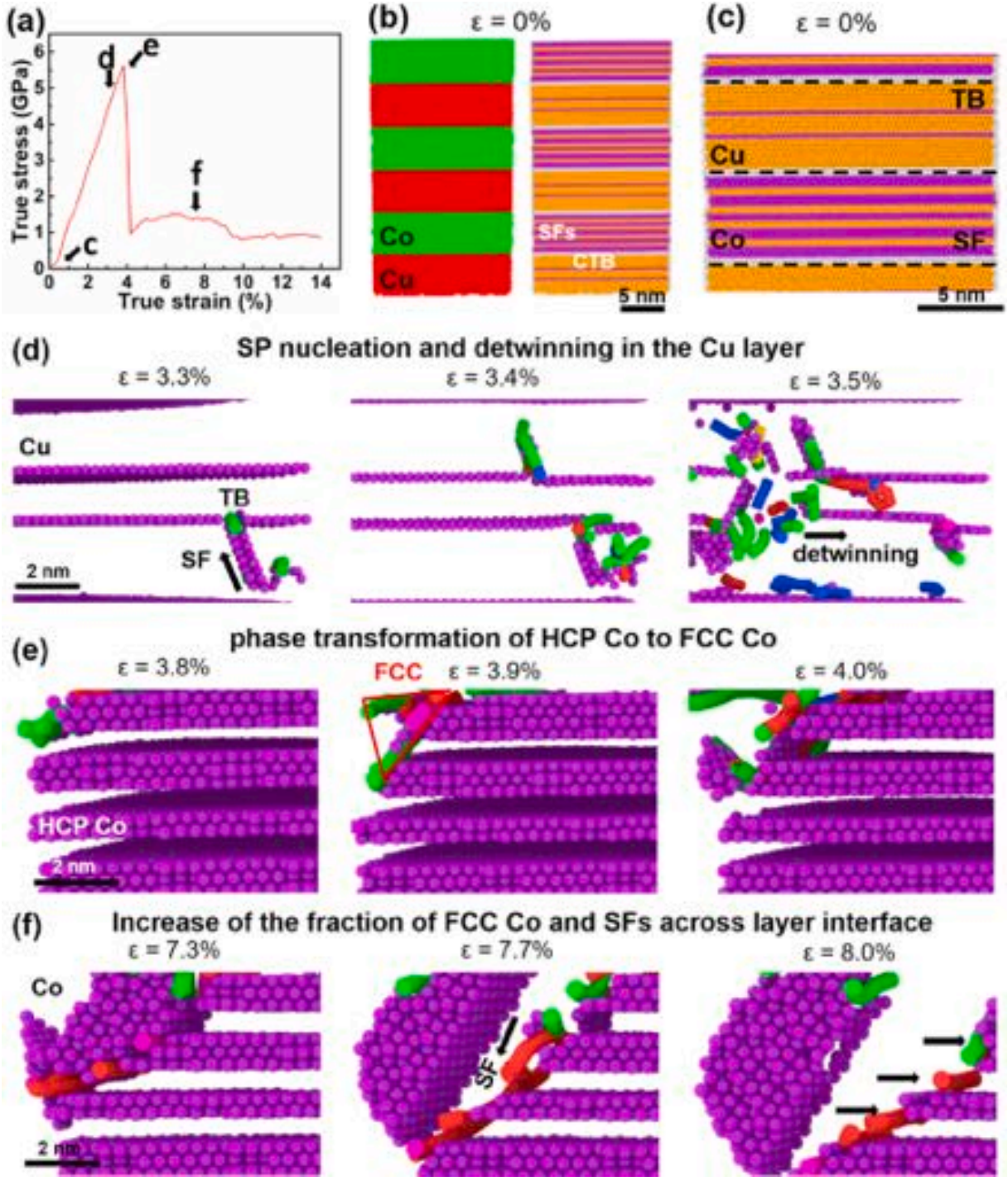

Fig. 16. MD simulation on the compression of FCC Cu (111)/HCP Co (0002) 5 nm nanopillars [55]. (a) The true stress-strain curve shows the pillar has a yield stress of 5.5 GPa. (b) Left panel shows Cu in red and Co in green. Right panel shows FCC and HCP structure in orange and purple color. (c) Cross-section view of the model system shows the pre-existing SFs in HCP Co and TBs in FCC Cu. (d) At 3.3-3.5% true strain, Shockley partials are nucleated and migrated along CTBs in the Cu layer, leading to detwinning. (e) Yielding occurs due to the HCP-to-FCC Co phase transformation at 3.8% strain. (f) Fraction of FCC Co increases rapidly during subsequent deformation. (For interpretation of the references to color in this figure legend, the reader is referred to the Web version of this article.)

tolerance of metallic materials. However, the role of SFs on radiation response of materials is largely unclear.

9. Conclusion

In this article, we reviewed recent studies on the SF mediated mechanical behaviors of various materials including nanostructured metallic materials, high entropy alloys and ceramics. These experimental and computational studies provide compelling evidence that high-density SFs can effectively strengthen materials by blocking dislocation migration and forming sessile dislocations at SF junctions. SFs also enable good ductility by emitting partial dislocations and promoting phase transformations during interactions with dislocations. However, there are still many unsolved issues that require further investigations, such as quantitative analysis of SF induced strengthening effect, phase transformation mechanism at atomistic level, high

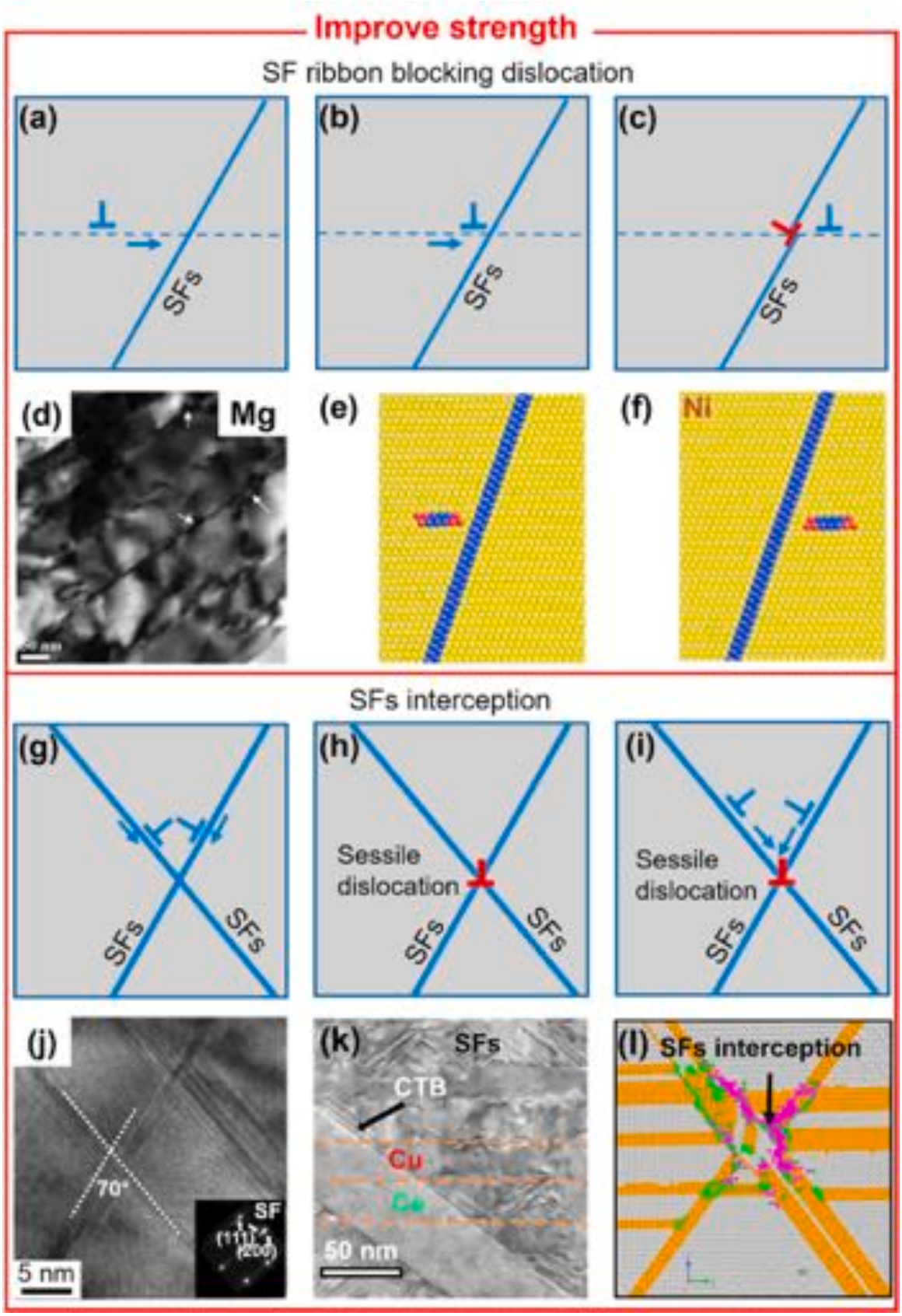

Fig. 17. The strengthening effect of SFs on mechanical behaviors. (a–c) Schematic shows SFs block the glide of dislocations on the inclined slip planes. (d) TEM evidence of SF blocking dislocation migration in HCP Mg [63]. (e–f) MD simulation shows a screw dislocation is blocked [106]. (g–i) Schematics showing SF interception and the sessile dislocation (at the intersection) block the glide of dislocations. (j) TEM micrograph shows the SFs ribbon interception (forming a Hirth lock) in FCC Co (100) [56]. (k) Inclined SFs in Co layer in Cu/Co (110) multilayers [55].(l) MD simulation shows partial dislocations are locked by the SF interceptions.

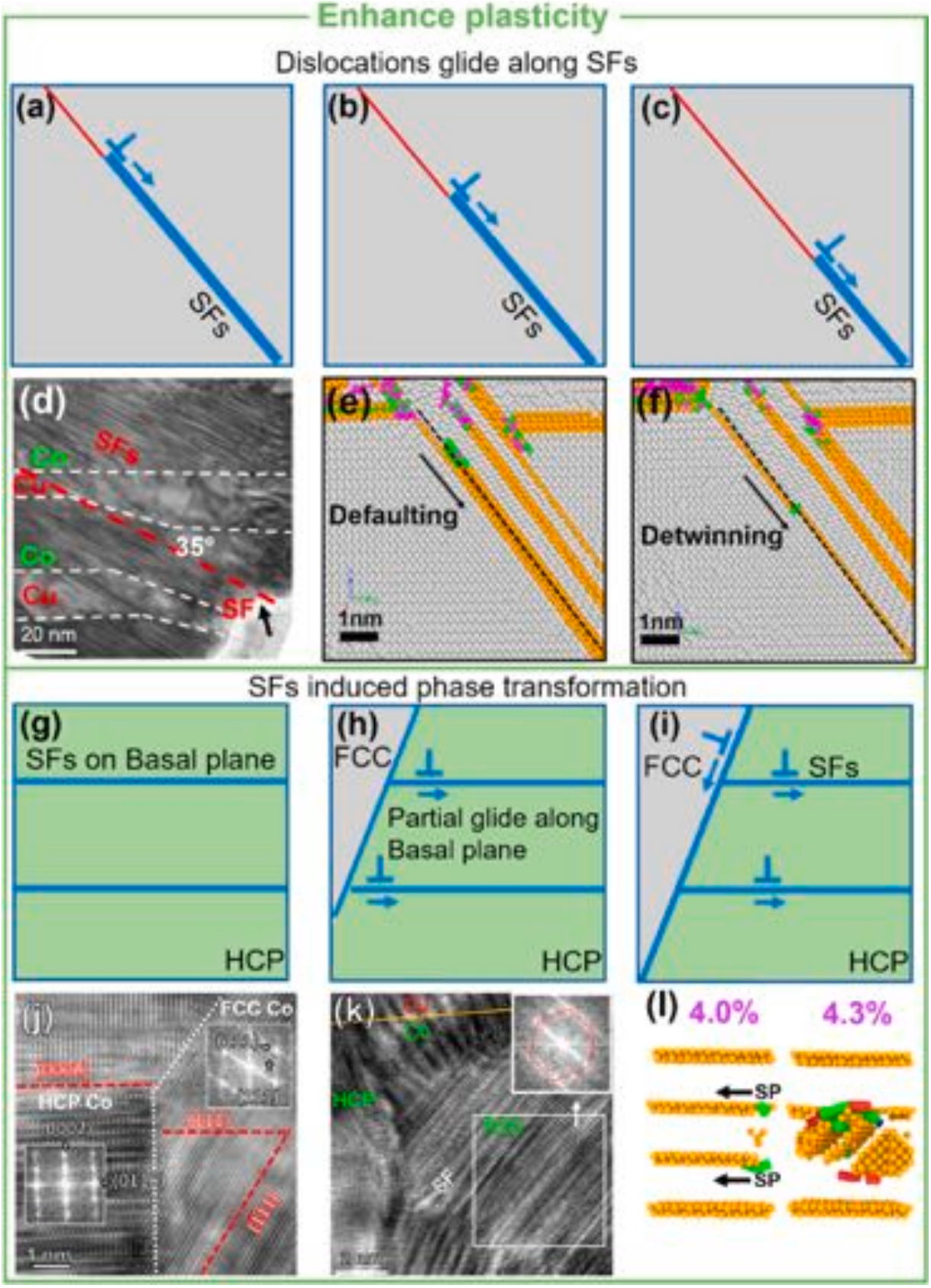

Fig. 18. The influence of SFs on plasticity (deformability). (a–c) A schematic shows a dislocation glide along the SF plane. (d) Partial dislocations glide along the inclined SFs in Cu/Co (110) multilayers and lead to shear bands. (e–f) MD simulation reveals partial dislocation glides along a SF, leading to defaulting and softening in FCC Co (100) [56]. (g–i) Schematics show SFs induced HCP-to-FCC phase transformation. (j) FCC Co formed in HCP Co during deformation accommodates the plastic deformation [54]. (k) HCP-to-FCC phase transformation in Cu (111)/Co (0002) 25 nm multilayers [55]. (l) SFs in HCP Co block the glide of dislocations and trigger the HCP-to-FCC phase transformation [54].

temperature stability, radiation stability and physical properties of materials.

Originality statement

This is a review article. We collected results from various published literature and performed thorough review on these results.

CRediT authorship contribution statement

Ruizhe Su: Writing - original draft, Data curation, collected literature data and prepared manuscript. **Dajla Neffati:** Writing - original draft, Data curation, collected literature data on MD simulation and wrote the simulation part of this manuscript. **Yifan Zhang:** Writing - original draft, wrote part of Chapter 7. **Jaehun Cho:** Writing - original draft, wrote part of Chapter 6. **Jin Li:** Writing - original draft, wrote part of Chapter 6. **Haiyan Wang:** Writing - review & editing, revised the manuscript. **Yashashree Kulkarni:** Writing - original draft, Data curation, collected literature data on MD simulation and wrote the simulation part of this manuscript. **Xinghang Zhang:** Writing - review & editing, designed manuscript structured and revised manuscript.

Declaration of competing interest

The authors declare that they have no known competing financial interests or personal relationships that could have appeared to influence the work reported in this paper.

Acknowledgments

RS and XZ acknowledge the financial support by NSF-DMR 1642759. DN and YK acknowledge the financial support by NSF-DMR 1508484. YZ is supported by DOE-BES under grant No. DE-SC0016337. HW, J.C. and X.Z. acknowledges the support from the U.S. Office of Naval Research (N00014-17-1-2087 and N00014-20-1-2043). Access to the Life Sciences Microscopy Center and Materials Science Microscopy Center at Purdue University are also acknowledged. The support from the Research Computing Data Core at the University of Houston is also acknowledged. We also acknowledge access to microscopy facilities at DOE Center for Integrated Nanotechnologies.

References

[1] L. Lu, Y. Shen, X. Chen, L. Qian, K. Lu, Ultrahigh strength and high electrical conductivity in copper, Science 304 (5669) (2004) 422–426.
[2] X. Zhang, A. Misra, H. Wang, M. Nastasi, J.D. Embury, T.E. Mitchell, R. G. Hoagland, J.P. Hirth, Nanoscale-twinning-induced strengthening in austenitic stainless steel thin films, Appl. Phys. Lett. 84 (7) (2004) 1096–1098.
[3] Y.F. Zhang, S. Xue, Q. Li, J. Li, J. Ding, T.J. Niu, R. Su, H. Wang, X. Zhang, Size dependent strengthening in high strength nanotwinned Al/Ti multilayers, Acta Mater. 175 (2019) 466–476.
[4] Y.F. Zhang, S. Xue, Q. Li, C. Fan, R. Su, J. Ding, H. Wang, H. Wang, X. Zhang, Microstructure and mechanical behavior of nanotwinned AlTi alloys with 9R phase, Scripta Mater. 148 (2018) 5–9.
[5] S. Xue, W. Kuo, Q. Li, Z. Fan, J. Ding, R. Su, H. Wang, X. Zhang, Texture-directed twin formation propensity in Al with high stacking fault energy, Acta Mater. 144 (2018) 226–234.
[6] Q. Li, S. Xue, J. Wang, S. Shao, A.H. Kwong, A. Giwa, Z. Fan, Y. Liu, Z. Qi, J. Ding, H. Wang, J.R. Greer, H. Wang, X. Zhang, High-strength nanotwinned Al alloys with 9R phase, Adv. Mater. 30 (11) (2018), 1704629.
[7] Q. Lu, Z. You, X. Huang, N. Hansen, L. Lu, Dependence of dislocation structure on orientation and slip systems in highly oriented nanotwinned Cu, Acta Mater. 127 (Supplement C) (2017) 85–97.
[8] J. Wang, X. Zhang, Twinning effects on strength and plasticity of metallic materials, MRS Bull. 41 (4) (2016) 274–281.
[9] D. Bufford, Y. Liu, J. Wang, H. Wang, X. Zhang, In situ nanoindentation study on plasticity and work hardening in aluminium with incoherent twin boundaries, Nat. Commun. 5 (2014) 4864.
[10] Y. Liu, J. Jian, Y. Chen, H. Wang, X. Zhang, Plasticity and ultra-low stress induced twin boundary migration in nanotwinned Cu by in situ nanoindentation studies, Appl. Phys. Lett. 104 (23) (2014), 231910.
[11] T.A. Furnish, A.M. Hodge, On the mechanical performance and deformation of nanotwinned Ag, Apl. Mater. 2 (4) (2014).
[12] N. Lu, K. Du, L. Lu, H.Q. Ye, Motion of 1/3 < 111 > dislocations on Sigma 3 {112} twin boundaries in nanotwinned copper, J. Appl. Phys. 115 (2) (2014).
[13] D. Bufford, H. Wang, X. Zhang, High strength, epitaxial nanotwinned Ag films, Acta Mater. 59 (1) (2011) 93–101.
[14] N. Li, J. Wang, A. Misra, X. Zhang, J.Y. Huang, J.P. Hirth, Twinning dislocation multiplication at a coherent twin boundary, Acta Mater. 59 (15) (2011) 5989–5996.
[15] N. Li, J. Wang, X. Zhang, A. Misra, In-situ TEM study of dislocation-twin boundaries interaction in nanotwinned Cu films, Jom 63 (9) (2011) 62–U62.
[16] X.H. Chen, L. Lu, K. Lu, Grain size dependence of tensile properties in ultrafine-grained Cu with nanoscale twins, Scripta Mater. 64 (4) (2011) 311–314.
[17] A. Singh, L. Tang, M. Dao, L. Lu, S. Suresh, Fracture toughness and fatigue crack growth characteristics of nanotwinned copper, Acta Mater. 59 (6) (2011) 2437–2446.
[18] Y.T. Zhu, X.L. Wu, X.Z. Liao, J. Narayan, L.J. Kecskés, S.N. Mathaudhu, Dislocation–twin interactions in nanocrystalline fcc metals, Acta Mater. 59 (2) (2011) 812–821.
[19] A. Stukowski, K. Albe, D. Farkas, Nanotwinned fcc metals: strengthening versus softening mechanisms, Phys. Rev. B 82 (22) (2010).
[20] J. Wang, N. Li, O. Anderoglu, X. Zhang, A. Misra, J.Y. Huang, J.P. Hirth, Detwinning mechanisms for growth twins in face-centered cubic metals, Acta Mater. 58 (6) (2010) 2262–2270.
[21] M. Bernardi, S.N. Raja, S.K. Lim, Nanotwinned gold nanowires obtained by chemical synthesis, Nanotechnology 21 (28) (2010), 285607.
[22] J.A. Brown, N.M. Ghoniem, Structure and motion of junctions between coherent and incoherent twin boundaries in copper, Acta Mater. 57 (15) (2009) 4454–4462.
[23] J. Wang, O. Anderoglu, J.P. Hirth, A. Misra, X. Zhang, Dislocation structures of Sigma 3 {112} twin boundaries in face centered cubic metals, Appl. Phys. Lett. 95 (2) (2009).
[24] Y. Kulkarni, R.J. Asaro, Are some nanotwinned fcc metals optimal for strength, ductility and grain stability? Acta Mater. 57 (16) (2009) 4835–4844.
[25] L. Lu, T. Zhu, Y. Shen, M. Dao, K. Lu, S. Suresh, Stress relaxation and the structure size-dependence of plastic deformation in nanotwinned copper, Acta Mater. 57 (17) (2009) 5165–5173.
[26] L. Lu, M. Dao, T. Zhu, J. Li, Size dependence of rate-controlling deformation mechanisms in nanotwinned copper, Scripta Mater. 60 (12) (2009) 1062–1066.
[27] Z.X. Wu, Y.W. Zhang, D.J. Srolovitz, Dislocation–twin interaction mechanisms for ultrahigh strength and ductility in nanotwinned metals, Acta Mater. 57 (15) (2009) 4508–4518.
[28] O. Anderoglu, A. Misra, H. Wang, X. Zhang, Thermal stability of sputtered Cu films with nanoscale growth twins, J. Appl. Phys. 103 (9) (2008), 094322.
[29] O. Anderoglu, A. Misra, H. Wang, F. Ronning, M.F. Hundley, X. Zhang, Epitaxial nanotwinned Cu films with high strength and high conductivity, Appl. Phys. Lett. 93 (8) (2008).
[30] Z.H. Jin, P. Gumbsch, K. Albe, E. Ma, K. Lu, H. Gleiter, H. Hahn, Interactions between non-screw lattice dislocations and coherent twin boundaries in face-centered cubic metals, Acta Mater. 56 (5) (2008) 1126–1135.
[31] F. Sansoz, H. Huang, D.H. Warner, An atomistic perspective on twinning phenomena in nano-enhanced fcc metals, Jom 60 (9) (2008) 79–84.
[32] Z.W. Shan, L. Lu, A.M. Minor, E.A. Stach, S.X. Mao, The effect of twin plane spacing on the deformation of copper containing a high density of growth twins, Jom 60 (9) (2008) 71–74.
[33] L.L. Shaw, A.L. Ortiz, J.C. Villegas, Hall-Petch relationship in a nanotwinned nickel alloy, Scripta Mater. 58 (11) (2008) 951–954.
[34] A.M. Hodge, Y.M. Wang, T.W. Barbee, Mechanical deformation of high-purity sputter-deposited nano-twinned copper, Scripta Mater. 59 (2) (2008) 163–166.
[35] K.A. Afanasyev, F. Sansoz, Strengthening in gold nanopillars with nanoscale twins, Nano Lett. 7 (7) (2007) 2056–2062.
[36] A.J. Cao, Y.G. Wei, Molecular dynamics simulation of plastic deformation of nanotwinned copper, J. Appl. Phys. 102 (8) (2007).
[37] Y.B. Wang, M.L. Sui, E. Ma, In situ observation of twin boundary migration in copper with nanoscale twins during tensile deformation, Phil. Mag. Lett. 87 (12) (2007) 935–942.
[38] X. Zhang, H. Wang, X.H. Chen, L. Lu, K. Lu, R.G. Hoagland, A. Misra, High-strength sputter-deposited Cu foils with preferred orientation of nanoscale growth twins, Appl. Phys. Lett. 88 (17) (2006).
[39] L. Lu, R. Schwaiger, Z.W. Shan, M. Dao, K. Lu, S. Suresh, Nano-sized twins induce high rate sensitivity of flow stress in pure copper, Acta Mater. 53 (7) (2005) 2169–2179.
[40] Y.M. Wang, T. Voisin, J.T. McKeown, J. Ye, N.P. Calta, Z. Li, Z. Zeng, Y. Zhang, W. Chen, T.T. Roehling, R.T. Ott, M.K. Santala, Philip J. Depond, M.J. Matthews, A.V. Hamza, T. Zhu, Additively manufactured hierarchical stainless steels with high strength and ductility, Nat. Mater. 17 (1) (2018) 63–71.
[41] T. Sinha, Y. Kulkarni, Alternating brittle and ductile response of coherent twin boundaries in nanotwinned metals, J. Appl. Phys. 116 (18) (2014).
[42] S. Jiao, Y. Kulkarni, Molecular dynamics study of creep mechanisms in nanotwinned metals, Comput. Mater. Sci. 110 (2015) 254–260.
[43] D. Chen, Y. Kulkarni, Elucidating the kinetics of twin boundaries from thermal fluctuations, MRS Communications 3 (4) (2013) 241.
[44] N. Li, J. Wang, J.Y. Huang, A. Misra, X. Zhang, Influence of slip transmission on the migration of incoherent twin boundaries in epitaxial nanotwinned Cu, Scripta Mater. 64 (2) (2011) 149–152.
[45] X. Li, Y. Wei, L. Lu, K. Lu, H. Gao, Dislocation nucleation governed softening and maximum strength in nano-twinned metals, Nature 464 (7290) (2010) 877–880.

[46] Z.H. Jin, P. Gumbsch, E. Ma, K. Albe, K. Lu, H. Hahn, H. Gleiter, The interaction mechanism of screw dislocations with coherent twin boundaries in different face-centred cubic metals, Scripta Mater. 54 (6) (2006) 1163–1168.
[47] P. Gu, M. Dao, Y. Zhu, Strengthening at nanoscaled coherent twin boundary in f.c.c. metals, Phil. Mag. 94 (11) (2014) 1249–1262.
[48] A.M. Hodge, T.A. Furnish, C.J. Shute, Y. Liao, X. Huang, C.S. Hong, Y.T. Zhu, T. W. Barbee Jr., J.R. Weertman, Twin stability in highly nanotwinned Cu under compression, torsion and tension, Scripta Mater. 66 (11) (2012) 872–877.
[49] Y.M. Wang, F. Sansoz, T. LaGrange, R.T. Ott, J. Marian, T.W. Barbee Jr., A. V. Hamza, Defective twin boundaries in nanotwinned metals, Nat. Mater. 12 (8) (2013) 697–702.
[50] E. Ma, Y.M. Wang, Q.H. Lu, M.L. Sui, L. Lu, K. Lu, Strain hardening and large tensile elongation in ultrahigh-strength nano-twinned copper, Appl. Phys. Lett. 85 (21) (2004) 4932–4934.
[51] R. Yuan, I.J. Beyerlein, C. Zhou, Statistical dislocation activation from grain boundaries and its role in the plastic anisotropy of nanotwinned copper, Acta Mater. 110 (2016) 8–18.
[52] A. Sedlmayr, E. Bitzek, D.S. Gianola, G. Richter, R. Mönig, O. Kraft, Existence of two twinning-mediated plastic deformation modes in Au nanowhiskers, Acta Mater. 60 (9) (2012) 3985–3993.
[53] L.-B. Han, Q. An, R.-S. Fu, L. Zheng, S.-N. Luo, Melting of defective Cu with stacking faults, J. Chem. Phys. 130 (2) (2009), 024508.
[54] R. Su, D. Neffati, J. Cho, Q. Li, J. Ding, H. Wang, Y. Kulkarni, X. Zhang, Phase transformation induced plasticity in high-strength hexagonal close packed Co with stacking faults, Scripta Mater. 173 (2019) 32–36.
[55] R. Su, D. Neffati, Q. Li, S. Xue, J. Cho, J. Li, J. Ding, Y. Zhang, C. Fan, H. Wang, Y. Kulkarni, X. Zhang, Ultra-high strength and plasticity mediated by partial dislocations and defect networks: Part I: texture effect, Acta Mater. (2019).
[56] R. Su, D. Neffati, S. Xue, Q. Li, Z. Fan, Y. Liu, H. Wang, Y. Kulkarni, X. Zhang, Deformation mechanisms in FCC Co dominated by high-density stacking faults, Mater. Sci. Eng., A 736 (2018) 12–21.
[57] Y. Liu, Y. Chen, K. Yu, H. Wang, J. Chen, X. Zhang, Stacking fault and partial dislocation dominated strengthening mechanisms in highly textured Cu/Co multilayers, Int. J. Plast. 49 (2013) 152–163.
[58] X. Feng, J. Zhang, K. Wu, X. Liang, G. Liu, J. Sun, Ultrastrong Al0.1CoCrFeNi high-entropy alloys at small scales: effects of stacking faults vs. nanotwins, Nanoscale 10 (28) (2018) 13329–13334.
[59] K. Wu, J.Y. Zhang, G. Li, Y.Q. Wang, J.C. Cui, G. Liu, J. Sun, Stacking fault-mediated ultrastrong nanocrystalline Ti thin films, Nanotechnology 28 (44) (2017), 445706.
[60] Z. Li, K.G. Pradeep, Y. Deng, D. Raabe, C.C. Tasan, Metastable high-entropy dual-phase alloys overcome the strength–ductility trade-off, Nature 534 (7606) (2016) 227–230.
[61] K. Youssef, M. Sakaliyska, H. Bahmanpour, R. Scattergood, C. Koch, Effect of stacking fault energy on mechanical behavior of bulk nanocrystalline Cu and Cu alloys, Acta Mater. 59 (14) (2011) 5758–5764.
[62] K. Ofei, L. Zhao, J. Sietsma, Microstructural development and deformation mechanisms during cold rolling of a medium stacking fault energy TWIP steel, J. Mater. Sci. Technol. 29 (2) (2013) 161–167.
[63] W.W. Jian, G.M. Cheng, W.Z. Xu, H. Yuan, M.H. Tsai, Q.D. Wang, C.C. Koch, Y. T. Zhu, S.N. Mathaudhu, Ultrastrong Mg alloy via nano-spaced stacking faults, Materials Research Letters 1 (2) (2013) 61–66.
[64] Z. Li, C.C. Tasan, K.G. Pradeep, D. Raabe, A TRIP-assisted dual-phase high-entropy alloy: grain size and phase fraction effects on deformation behavior, Acta Mater. 131 (2017) 323–335.
[65] X. Wu, N. Tao, Y. Hong, G. Liu, B. Xu, J. Lu, K.J.A.M. Lu, Strain-induced grain refinement of cobalt during surface mechanical attrition treatment 53 (3) (2005) 681–691.
[66] X. Wu, N. Tao, Y. Hong, J. Lu, K. Lu, γ→ε martensite transformation and twinning deformation in fcc cobalt during surface mechanical attrition treatment, Scripta Mater. 52 (7) (2005) 547–551.
[67] X.Z. Liao, Y.H. Zhao, S.G. Srinivasan, Y.T. Zhu, R.Z. Valiev, D.V. Gunderov, Deformation twinning in nanocrystalline copper at room temperature and low strain rate, Appl. Phys. Lett. 84 (4) (2004) 592–594.
[68] X. Wu, Y.T. Zhu, M.W. Chen, E. Ma, Twinning and stacking fault formation during tensile deformation of nanocrystalline Ni, Scripta Mater. 54 (9) (2006) 1685–1690.
[69] W.W. Jian, G.M. Cheng, W.Z. Xu, C.C. Koch, Q.D. Wang, Y.T. Zhu, S. N. Mathaudhu, Physics and model of strengthening by parallel stacking faults, Appl. Phys. Lett. 103 (13) (2013), 133108.
[70] S. Sandlöbes, M. Friák, S. Zaefferer, A. Dick, S. Yi, D. Letzig, Z. Pei, L.F. Zhu, J. Neugebauer, D. Raabe, The relation between ductility and stacking fault energies in Mg and Mg–Y alloys, Acta Mater. 60 (6–7) (2012) 3011–3021.
[71] B. Smola, I. Stulıková, J. Pelcova, B. Mordike, Significance of stable and metastable phases in high temperature creep resistant magnesium–rare earth base alloys, J. Alloys Compd. 378 (1–2) (2004) 196–201.
[72] M. Wang, Z. Li, D. Raabe, In-situ SEM observation of phase transformation and twinning mechanisms in an interstitial high-entropy alloy, Acta Mater. 147 (2018) 236–246.
[73] F. He, Z. Wang, Q. Wu, D. Chen, T. Yang, J. Li, J. Wang, C.T. Liu, J.-j. Kai, Tuning the defects in face centered cubic high entropy alloy via temperature-dependent stacking fault energy, Scripta Mater. 155 (2018) 134–138.
[74] B. Cai, B. Liu, S. Kabra, Y. Wang, K. Yan, P.D. Lee, Y. Liu, Deformation mechanisms of Mo alloyed FeCoCrNi high entropy alloy: in situ neutron diffraction, Acta Mater. 127 (2017) 471–480.
[75] J. Liu, C. Chen, Y. Xu, S. Wu, G. Wang, H. Wang, Y. Fang, L. Meng, Deformation twinning behaviors of the low stacking fault energy high-entropy alloy: an in-situ TEM study, Scripta Mater. 137 (2017) 9–12.
[76] A.J. Zaddach, C. Niu, C.C. Koch, D.L. Irving, Mechanical properties and stacking fault energies of NiFeCrCoMn high-entropy alloy, JOM 65 (12) (2013) 1780–1789.
[77] F. Otto, A. Dlouhý, C. Somsen, H. Bei, G. Eggeler, E.P. George, The influences of temperature and microstructure on the tensile properties of a CoCrFeMnNi high-entropy alloy, Acta Mater. 61 (15) (2013) 5743–5755.
[78] X. Zhang, A. Misra, H. Wang, T. Shen, M. Nastasi, T. Mitchell, J. Hirth, R. Hoagland, J. Embury, Enhanced hardening in Cu/330 stainless steel multilayers by nanoscale twinning, Acta Mater. 52 (4) (2004) 995–1002.
[79] J. Cho, Y. Li, Z. Shang, J. Li, Q. Li, H. Wang, Y. Wu, X. Zhang, Extrinsic size dependent plastic deformability of ZnS micropillars, Mater. Sci. Eng., A 792 (2020), 139706.
[80] J. Li, J. Cho, J. Ding, H. Charalambous, S. Xue, H. Wang, X.L. Phuah, J. Jian, X. Wang, C. Ophus, T. Tsakalakos, R.E. García, A.K. Mukherjee, N. Bernstein, C. S. Hellberg, H. Wang, X. Zhang, Nanoscale stacking fault–assisted room temperature plasticity in flash-sintered TiO_2, Science Advances 5 (9) (2019) eaaw5519.
[81] J. Cho, Q. Li, H. Wang, Z. Fan, J. Li, S. Xue, K.S.N. Vikrant, H. Wang, T.B. Holland, A.K. Mukherjee, R.E. García, X. Zhang, High temperature deformability of ductile flash-sintered ceramics via in-situ compression, Nat. Commun. 9 (1) (2018) 2063.
[82] J. Luo, The scientific questions and technological opportunities of flash sintering: from a case study of ZnO to other ceramics, Scripta Mater. 146 (2018) 260–266.
[83] R. Todd, E. Zapata-Solvas, R. Bonilla, T. Sneddon, P. Wilshaw, Electrical characteristics of flash sintering: thermal runaway of Joule heating, J. Eur. Ceram. Soc. 35 (6) (2015) 1865–1877.
[84] J. Narayan, A new mechanism for field-assisted processing and flash sintering of materials, Scripta Mater. 69 (2) (2013) 107–111.
[85] X. Zhang, A. Misra, H. Wang, A.L. Lima, M.F. Hundley, R.G. Hoagland, Effects of deposition parameters on residual stresses, hardness and electrical resistivity of nanoscale twinned 330 stainless steel thin films, J. Appl. Phys. 97 (9) (2005).
[86] X.H. Chen, L. Lu, Work hardening of ultrafine-grained copper with nanoscale twins, Scripta Mater. 57 (2) (2007) 133–136.
[87] B. Li, B.Y. Cao, K.T. Ramesh, E. Ma, A nucleation mechanism of deformation twins in pure aluminum, Acta Mater. 57 (15) (2009) 4500–4507.
[88] O. Anderoglu, A. Misra, J. Wang, R.G. Hoagland, J.P. Hirth, X. Zhang, Plastic flow stability of nanotwinned Cu foils, Int. J. Plast. 26 (6) (2010) 875–886.
[89] A.M. Hodge, T.A. Furnish, A.A. Navid, T.W. Barbee Jr., Shear band formation and ductility in nanotwinned Cu, Scripta Mater. 65 (11) (2011) 1006–1009.
[90] D. Bufford, Z. Bi, Q.X. Jia, H. Wang, X. Zhang, Nanotwins and stacking faults in high-strength epitaxial Ag/Al multilayer films, Appl. Phys. Lett. 101 (22) (2012).
[91] D. Bufford, H. Wang, X. Zhang, Thermal stability of twins and strengthening mechanisms in differently oriented epitaxial nanotwinned Ag films, J. Mater. Res. 28 (13) (2013) 1729–1739.
[92] D. Bufford, Y. Liu, Y. Zhu, Z. Bi, Q.X. Jia, H. Wang, X. Zhang, formation mechanisms of high-density growth twins in aluminum with high stacking-fault energy, Materials Research Letters 1 (1) (2013) 51–60.
[93] J. Li, Y. Chen, S. Xue, H. Wang, X. Zhang, Comparison of size dependent strengthening mechanisms in Ag/Fe and Ag/Ni multilayers, Acta Mater. 114 (2016) 154–163.
[94] M. Lentz, M. Risse, N. Schaefer, W. Reimers, I.J. Beyerlein, Strength and ductility with {10(1)over-bar1} - {10(1)over-bar2} double twinning in a magnesium alloy, Nat. Commun. 7 (2016) 7.
[95] M. Ardeljan, I.J. Beyerlein, M. Knezevic, Effect of dislocation density-twin interactions on twin growth in AZ31 as revealed by explicit crystal plasticity finite element modeling, Int. J. Plast. 99 (2017) 81–101.
[96] S. Zheng, I.J. Beyerlein, J.S. Carpenter, K. Kang, J. Wang, W. Han, N.A. Mara, High-strength and thermally stable bulk nanolayered composites, due to twin-induced interfaces 4 (2013) 1696.
[97] F. Sansoz, K. Lu, T. Zhu, A. Misra, Strengthening and plasticity in nanotwinned metals, MRS Bull. 41 (4) (2016) 292–297.
[98] Z. Zeng, X. Li, L. Lu, T. Zhu, Fracture in a thin film of nanotwinned copper, Acta Mater. 98 (2015) 313–317.
[99] A. Kobler, T. Beuth, T. Klöffel, R. Prang, M. Moosmann, T. Scherer, S. Walheim, H. Hahn, C. Kübel, B. Meyer, T. Schimmel, E. Bitzek, Nanotwinned silver nanowires: structure and mechanical properties, Acta Mater. 92 (Supplement C) (2015) 299–308.
[100] J.R. Greer, W.D. Nix, Nanoscale gold pillars strengthened through dislocation starvation, Phys. Rev. B 73 (24) (2006), 245410.
[101] A.T. Jennings, J. Li, J.R. Greer, Emergence of strain-rate sensitivity in Cu nanopillars: transition from dislocation multiplication to dislocation nucleation, Acta Mater. 59 (14) (2011) 5627–5637.
[102] J.Y. Zhang, G. Liu, J. Sun, Strain rate effects on the mechanical response in multi- and single-crystalline Cu micropillars: grain boundary effects, Int. J. Plast. 50 (2013) 1–17.
[103] Z.W. Shan, R.K. Mishra, S.A.S. Asif, O.L. Warren, A.M. Minor, Mechanical annealing and source-limited deformation in submicrometre-diameter Ni crystals, Nat. Mater. 7 (2) (2008) 115–119.
[104] Z.-J. Wang, Q.-J. Li, Z.-W. Shan, J. Li, J. Sun, E. Ma, Sample size effects on the large strain bursts in submicron aluminum pillars, Appl. Phys. Lett. 100 (7) (2012), 071906.
[105] F.F. Csikor, C. Motz, D. Weygand, M. Zaiser, S. Zapperi, Dislocation avalanches, strain bursts, and the problem of plastic forming at the micrometer scale, Science 318 (5848) (2007) 251–254.

[106] H. Wei, Y. Wei, Interaction between a screw dislocation and stacking faults in FCC metals, Mater. Sci. Eng., A 541 (2012) 38–44.
[107] D.B. Miracle, O.N. Senkov, A critical review of high entropy alloys and related concepts, Acta Mater. 122 (2017) 448–511.
[108] Z. Zhang, M.M. Mao, J. Wang, B. Gludovatz, Z. Zhang, S.X. Mao, E.P. George, Q. Yu, R.O. Ritchie, Nanoscale origins of the damage tolerance of the high-entropy alloy CrMnFeCoNi, Nat. Commun. 6 (1) (2015) 10143.
[109] Z. Wu, C.M. Parish, H. Bei, Nano-twin mediated plasticity in carbon-containing FeNiCoCrMn high entropy alloys, J. Alloys Compd. 647 (2015) 815–822.
[110] A.J. Zaddach, R.O. Scattergood, C.C. Koch, Tensile properties of low-stacking fault energy high-entropy alloys, Mater. Sci. Eng., A 636 (2015) 373–378.
[111] Y. Zhang, T.T. Zuo, Z. Tang, M.C. Gao, K.A. Dahmen, P.K. Liaw, Z.P. Lu, Microstructures and properties of high-entropy alloys, Prog. Mater. Sci. 61 (2014) 1–93.
[112] S.-Y. Chang, M.-K. Chen, D.-S. Chen, Multiprincipal-element AlCrTaTiZr-nitride nanocomposite film of extremely high thermal stability as diffusion barrier for Cu metallization, J. Electrochem. Soc. 156 (5) (2009) G37–G42.
[113] Y. Zhang, X. Yang, P. Liaw, Alloy design and properties optimization of high-entropy alloys, Jom 64 (7) (2012) 830–838.
[114] X. Yang, Y. Zhang, P. Liaw, Microstructure and compressive properties of NbTiVTaAlx high entropy alloys, Procedia Engineering 36 (2012) 292–298.
[115] J.W. Yeh, S.K. Chen, S.J. Lin, J.Y. Gan, T.S. Chin, T.T. Shun, C.H. Tsau, S. Y. Chang, Nanostructured high-entropy alloys with multiple principal elements: novel alloy design concepts and outcomes, Adv. Eng. Mater. 6 (5) (2004) 299–303.
[116] L. Lu, X. Chen, X. Huang, K. Lu, Revealing the maximum strength in nanotwinned copper, Science 323 (5914) (2009) 607–610.
[117] X. Gao, Y. Lu, B. Zhang, N. Liang, G. Wu, G. Sha, J. Liu, Y. Zhao, Microstructural origins of high strength and high ductility in an AlCoCrFeNi2.1 eutectic high-entropy alloy, Acta Mater. 141 (2017) 59–66.
[118] Z. Li, C.C. Tasan, H. Springer, B. Gault, D. Raabe, Interstitial atoms enable joint twinning and transformation induced plasticity in strong and ductile high-entropy alloys, Sci. Rep. 7 (1) (2017), 40704.
[119] J. Cho, Q. Li, H. Wang, Z. Fan, J. Li, S. Xue, K.S.N. Vikrant, H. Wang, T.B. Holland, A.K. Mukherjee, R.E. Garcia, X. Zhang, High temperature deformability of ductile flash-sintered ceramics via in-situ compression, Nat. Commun. 9 (2018).
[120] Z. Du, X.M. Zeng, Q. Liu, C.A. Schuh, C.L. Gan, Superelasticity in micro-scale shape memory ceramic particles, Acta Mater. 123 (2017) 255–263.
[121] S. Korte, W.J. Clegg, Micropillar compression of ceramics at elevated temperatures, Scripta Mater. 60 (9) (2009) 807–810.
[122] M. Belmonte, Advanced ceramic materials for high temperature applications, Adv. Eng. Mater. 8 (8) (2006) 693–703.
[123] M. Cain, R. Morrell, Nanostructured ceramics: a review of their potential, Appl. Organomet. Chem. 15 (5) (2001) 321–330.
[124] G.N. Morscher, P. Pirouz, A.H. Heuer, TEMPERATURE-DEPENDENCE OF hardness IN yttria-stabilized zirconia single-crystals, J. Am. Ceram. Soc. 74 (3) (1991) 491–500.
[125] D.B. Miracle, H.A. Lipsitt, MECHANICAL-PROPERTIES OF fine-grained substoichiometric titanium carbide, J. Am. Ceram. Soc. 66 (8) (1983) 592–597.
[126] R.J. Stokes, C.H. Li, Dislocations and the tensile strength OF magnesium oxide, J. Am. Ceram. Soc. 46 (9) (1963) 423–434.
[127] J. Nie, Y. Zhang, J.M. Chan, S. Jiang, R. Huang, J. Luo, Two-step flash sintering of ZnO: fast densification with suppressed grain growth, Scripta Mater. 141 (2017) 6–9.
[128] S.K. Jha, K. Terauds, J.-M. Lebrun, R. Raj, Beyond flash sintering in 3 mol % yttria stabilized zirconia, J. Ceram. Soc. Jpn. 124 (4) (2016) 283–288.
[129] H. Charalambous, S.K. Jha, K.H. Christian, R.T. Lay, T. Tsakalakos, Flash sintering using controlled current ramp, J. Eur. Ceram. Soc. 38 (10) (2018) 3689–3693.
[130] J. Li, L. Guan, W. Zhang, M. Luo, J. Song, X. Song, S. An, Sintering behavior of samarium doped ceria under DC electrical field, Ceram. Int. 44 (2) (2018) 2470–2477.
[131] Y. Zhang, J. Nie, J.M. Chan, J. Luo, Probing the densification mechanisms during flash sintering of ZnO, Acta Mater. 125 (2017) 465–475.
[132] Y. Zhang, J.-I. Jung, J. Luo, Thermal runaway, flash sintering and asymmetrical microstructural development of ZnO and ZnO-Bi2O3 under direct currents, Acta Mater. 94 (2015) 87–100.
[133] Y. Zhang, J. Luo, Promoting the flash sintering of ZnO in reduced atmospheres to achieve nearly full densities at furnace temperatures of < 120 degrees C, Scripta Mater. 106 (2015) 26–29.
[134] S.K. Jha, R. Raj, The effect of electric field on sintering and electrical conductivity of titania, J. Am. Ceram. Soc. 97 (2) (2014) 527–534.
[135] M.C. Steil, D. Marinha, Y. Aman, J.R.C. Gomes, M. Kleitz, From conventional ac flash-sintering of YSZ to hyper-flash and double flash, J. Eur. Ceram. Soc. 33 (11) (2013) 2093–2101.
[136] J.C. M'Peko, J.S.C. Francis, R. Raj, Impedance spectroscopy and dielectric properties of flash versus conventionally sintered yttria-doped zirconia electroceramics viewed at the microstructural level, J. Am. Ceram. Soc. 96 (12) (2013) 3760–3767.
[137] M. Cologna, J.S.C. Francis, R. Raj, Field assisted and flash sintering of alumina and its relationship to conductivity and MgO-doping, J. Eur. Ceram. Soc. 31 (15) (2011) 2827–2837.
[138] M. Cologna, B. Rashkova, R. Raj, Flash sintering of nanograin zirconia in < 5 s at 850 degrees C, J. Am. Ceram. Soc. 93 (11) (2010) 3556–3559.
[139] H. Wang, X.L. Phuah, H. Charalambous, S.K. Jha, J. Li, T. Tsakalakos, X. Zhang, H. Wang, Staged microstructural study of flash sintered titania, Materialia 8 (2019), 100451.
[140] J. Kwon, A.A. Sharma, J.A. Bain, Y.N. Picard, M. Skowronski, Oxygen vacancy creation, drift, and aggregation in TiO2-based resistive switches at low temperature and voltage, Adv. Funct. Mater. 25 (19) (2015) 2876–2883.
[141] E. Karaksina, T. Gracheva, D. Shevarenkov, Structural defects in CVD ZnS, Inorg. Mater. 46 (1) (2010) 6–10.
[142] E. Omurzak, T. Mashimo, S. Sulaimankulova, S. Takebe, L. Chen, Z. Abdullaeva, C. Iwamoto, Y. Oishi, H. Ihara, H. Okudera, Wurtzite-type ZnS nanoparticles by pulsed electric discharge, Nanotechnology 22 (36) (2011) 365602.
[143] Y.F. Zhang, Q. Li, M. Gong, S. Xue, J. Ding, J. Li, J. Cho, T. Niu, R. Su, N. A. Richter, H. Wang, J. Wang, X. Zhang, Deformation behavior and phase transformation of nanotwinned Al/Ti multilayers, Appl. Surf. Sci. (2020), 146776.
[144] I. Knorr, N.M. Cordero, E.T. Lilleodden, C.A. Volkert, Mechanical behavior of nanoscale Cu/PdSi multilayers, Acta Mater. 61 (13) (2013) 4984–4995.
[145] D. Bhattacharyya, N.A. Mara, P. Dickerson, R.G. Hoagland, A. Misra, Compressive flow behavior of Al-TiN multilayers at nanometer scale layer thickness, Acta Mater. 59 (10) (2011) 3804–3816.
[146] R.L. Schoeppner, J.M. Wheeler, J. Zechner, J. Michler, H.M. Zbib, D.F. Bahr, Coherent interfaces increase strain-hardening behavior in tri-component nano-scale metallic multilayer thin films, Materials Research Letters 3 (2) (2015) 114–119.
[147] P. Dayal, M.Z. Quadir, C. Kong, N. Savvides, M. Hoffman, Transition from dislocation controlled plasticity to grain boundary mediated shear in nanolayered aluminum/palladium thin films, Thin Solid Films 519 (10) (2011) 3213–3220.
[148] W. Guo, E. Jägle, J. Yao, V. Maier, S. Korte-Kerzel, J.M. Schneider, D. Raabe, Intrinsic and extrinsic size effects in the deformation of amorphous CuZr/nanocrystalline Cu nanolaminates, Acta Mater. 80 (Supplement C) (2014) 94–106.
[149] N.A. Mara, D. Bhattacharyya, P. Dickerson, R.G. Hoagland, A. Misra, Deformability of ultrahigh strength 5 nm Cu/Nb nanolayered composites, Appl. Phys. Lett. 92 (23) (2008).
[150] N. Li, N.A. Mara, Y.Q. Wang, M. Nastasi, A. Misra, Compressive flow behavior of Cu thin films and Cu/Nb multilayers containing nanometer-scale helium bubbles, Scripta Mater. 64 (10) (2011) 974–977.